To the Graduate Council:

I am submitting herewith a thesis written by Harry James Kowal, entitled "Analyzing the Flow Characteristics of a Fluid Oscillator." I have examined the final copy of this thesis for form and content and recommend that it be accepted in partial fulfillment of the requirements for the degree of Master of Science, with a major in Aerospace Engineering.

Ahmad D. Vakili, Major Professor

We have read this thesis
and recommend its acceptance:

Accepted for the Council:

Vice Provost
and Dean of The Graduate School

STATEMENT OF PERMISSION TO USE

In presenting this thesis in partial fulfillment of the requirements for a Master's degree at the University of Tennessee, Knoxville, I agree that the library shall make it available to borrowers under rules of the library. Brief quotations from this thesis are allowable without special permission, provided that accurate acknowledgment of the source is made.

Permission for extensive quotation from or reproduction of this thesis may be granted by my major professor, or in his absence, by the Head of Interlibrary Services when, in the opinion of either, the proposed use of the material is for scholarly purposes. Any copying or use of the material in this thesis for financial gain shall not be allowed without my written permission.

Signature ____________________

Date 23 July 1990

ANALYZING THE FLOW CHARACTERISTICS OF A FLUIDIC OSCILLATOR

A Thesis

Presented for the

Master of Science

Degree

The University of Tennessee, Knoxville

Harry James Kowal

August 1990

ACKNOWLEDGMENTS

This paper represents the culmination of two years intense academic work. For my family, this meant long days, late hours and missed holidays. Throughout it all, my devoted wife, Cheryl, continually provided me with endless support and encouragement. Her patience and understanding gave me the strength and motivation to succeed. This thesis is dedicated to Cheryl in appreciation for all her efforts that made it possible.

I would like to thank my academic advisor, Dr. Ahmad Vakili, for his advice and guidance throughout my studies at UTSI. I would, also, like to thank Dr. Roger Crawford for his continued support and especially for his efforts in writing my military assessments. I am, indeed, indebted to all the members of my committee, Dr. Vakili, Dr. Crawford, and Dr. Wu for their guidance and support during my experimentations and while preparing my thesis. A special thanks to my colleague, Christian Gauthier, whose assistance and competitive spirit enhanced our level of understanding.

I would like to express my sincere appreciation to the technicians in the lab, Harold Sartain, Ricky Meeker, Dick Ray, and Jim Boazman for their assistance throughout the experimental proceedings. I would like to thank Loyd Lester and his crew for their excellent workmanship in constructing the test model.

ABSTRACT

The research performed in this thesis concentrated on the design and analysis of a fluidic oscillator for the provision of a continuously pulsed output. Wall attachment theory was used as the basis for design specifications. A plexiglas model was constructed and tested in the University of Tennessee Space Institute water tunnel. Qualitative appreciation of the flow characteristics was gained using dye injection as a method of flow visualization. A second model was machined out of aluminum for testing with air. Quantitative measurements of the flow parameters were obtained with various instrumentation while a qualitative assessment of the flow was performed using surface oil flow visualization technique.

The overall results indicate that fluidic oscillators may be used as a source of unsteady flow. This study confirmed that frequency of oscillation is a linear function of supply flow rate for water and air under non-choked nozzle conditions. The design tested in this study did, however, demonstrate unacceptable total pressure losses. Further research into different design configurations is recommended.

TABLE OF CONTENTS

LIST OF FIGURES

FIGURE PAGE

NOMENCLATURE

b	- Power nozzle width
B	- Offset distance from nozzle to side wall
J	- Power jet momentum flux per unit height
J_1	- Momentum flux per unit height moving downstream
J_2	- Momentum flux per unit height into the separation bubble
q_c	- Control flow rate
q_e	- Entrained flow rate
q_r	- Return flow rate
q_{sup}	- Supply flow rate
R	- Radius of jet curvature
s	- Distance along curved jet centerline
s_2	- Distance along curved jet centerline to wall attachment point
u	- Jet velocity
x_R	- Distance along wall to attachment point
y	- Dimension perpendicular to jet axis
y_A	- Value of y corresponding to the attachment streamline
α	- Angle of inclination of the attachment wall
θ	- Angle extended jet centerline makes with the attachment wall
ρ	- Density
σ_e	- Spread factor

CHAPTER I

INTRODUCTION

Background

In an effort to advance aerospace technology, researchers have devoted much time in developing efficient propulsion methods for aircraft to fly faster and farther. One of these efforts has been concentrated on the Supersonic Combustion Ramjet (or Scramjet). A major problem in its development has been achieving a high combustion efficiency. The problem stems from the inability to gain adequate mixing between fuel and oxidizer by conventional techniques. If the fuel is introduced as a constant cross jet into the supersonic flow field, the resultant shock wave complicates the situation further and imposes unacceptable heat transfer conditions to the surrounding materials. Vakili et. al.[1], however, has successfully demonstrated the enhanced mixing characteristics of supplying a pulsating cross jet into a subsonic flow. It is envisaged that this same result is possible if the pulsating input is provided to a supersonic cross flow.

To compliment this approach to the design of a supersonic combustion chamber, the requirement for a device that produces a continuous pulsating flow becomes evident. In keeping with the need for an efficient and reliable device, the focus of this thesis is the design and analysis of a fluidic oscillator with no moving parts for the provision of a pulsing output.

Fluidics

During the 1960's, fluidics gained an enormous amount of attention for their ability to control forces. To date, significant research has been done in the area of fluidics and a large variety of fluidic devices have been built. Fluidics have been used as amplifiers, logic devices as well as oscillators. Unfortunately, the onset of electronic components, which are distinctively smaller and faster, diminished the level of interest in fluidics. Modern technology, however, has created many different environments which favor the use of fluidics and their ability to withstand severe temperatures, high vibrations, mechanical and thermal shocks, as well as their inherent capability to withstand hostile electronic countermeasures. Thus, fluidics have, once again, found application in current technological advancement. Beale and Lawler[2] have developed a wall-attachment fluidic oscillator for application as a flow metering device. As well, S. M. Riddlebaugh[3] has presented a study of a fluidic oscillator to measure fuel-air ratios of combustion gases.

Statement of Objective

The research in this thesis concentrates on the design and analysis of a fluidic oscillator with no moving parts for the provision of a pulsed output. This study is divided into four main sections. The first section provides a brief introduction into the theoretical background upon which the operation of a fluidic oscillator is based. This is followed by the qualitative analysis of a plexiglas model in a water tunnel. The next section analyzes the performance characteristics of an aluminum model when it is operated with air as the medium. Finally, the results and conclusions are discussed in the last section.

CHAPTER II

TECHNICAL REVIEW

Wall-Attachment Devices

The Coanda effect is the fundamental principle that governs the operation of wall-attachment fluidic devices. The effect is named after Henri Coanda who, in 1932, was the first to observe that a free jet emerging from a nozzle tends to follow a nearby surface. The flow attaches itself to the surface if the curvature or angle of inclination of the surface is not too great. The phenomenon is explained through the process of entrainment. When the free jet emanates from the orifice, nearby fluid particles are entrained. If the flow is close to a solid surface, the amount of fluid particles is limited and a low pressure region is developed. The jet consequently moves toward the low pressure region. As illustrated in Figure 2.1, when the jet becomes attached to the surface, the low pressure region becomes closed. This area is called a separation bubble. Particles are continually entrained from the separation bubble by the jet but are, also, replenished by the jet near the point of wall attachment. Whether or not the separation bubble remains depends on the rate of particle depletion versus the rate of their replenishment.

To be able to control or switch the jet attachment from one surface to another, a configuration as presented in Figure 2.2 can be employed. Considering the supply jet attached to the left boundary, the output flow results through Channel 01. To change this condition, positive pressure is applied to Control C1, increasing the pressure within the separation bubble. When the pressure inside the separation bubble exceeds that on the other side of the jet, the jet detaches itself from the left boundary wall and re-attaches itself to the right. The output results through

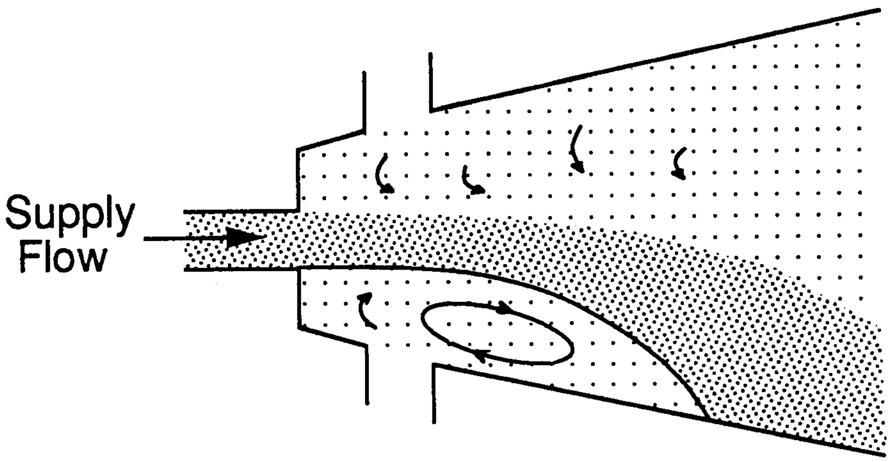

Figure 2.1. Coanda Effect.

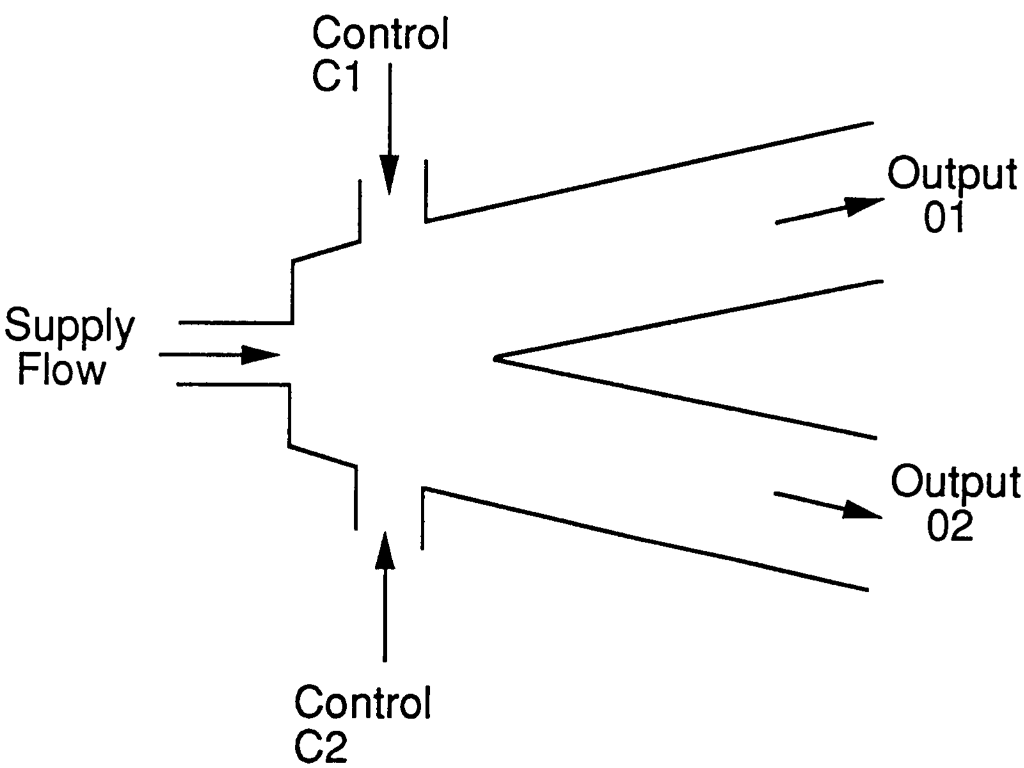

Figure 2.2. Bistable Wall Reattachment Device.

Channel 02. Switching the jet back to the left boundary wall necessitates a similar control flow through Control C2.

The attachment of the jet can be made to oscillate continuously between walls by the use of feedback loops. Referring to Figure 2.3, as the flow is attached to one side of the element, its momentum forces some of the flow into the feedback loop. This results in a pressure pulse being transmitted through the feedback loop to the separation bubble. When the pulse is large enough, the jet is forced to the opposite wall. A similar process now occurs on the opposite side of the device and a sustained oscillation results. It has been shown that the frequency of oscillation is determined by the following factors;

a. The time required for the fluid to flow back through the feedback loop;
b. The time required for the control jet pressure to produce wall separation; and
c. The delay time required for the fluid to traverse the distance between the walls.

The work performed by W.H. Delashmit, Jr.[4], concludes that in order to increase the frequency of oscillation, the flow volume of the feedback loops should be decreased. A linear relationship between oscillation frequency and inverse feedback loop flow volume has been demonstrated. In Beale and Lawler's[2] hydrodynamic study of a wall-attachment fluidic oscillator applied to volume flow metering, the results show that frequency of oscillation is a linear function of fluid supply flow rate. A further conclusion of the study shows that the pressure drop across the oscillator is, also, proportional to the supply flow rate. The experiments performed

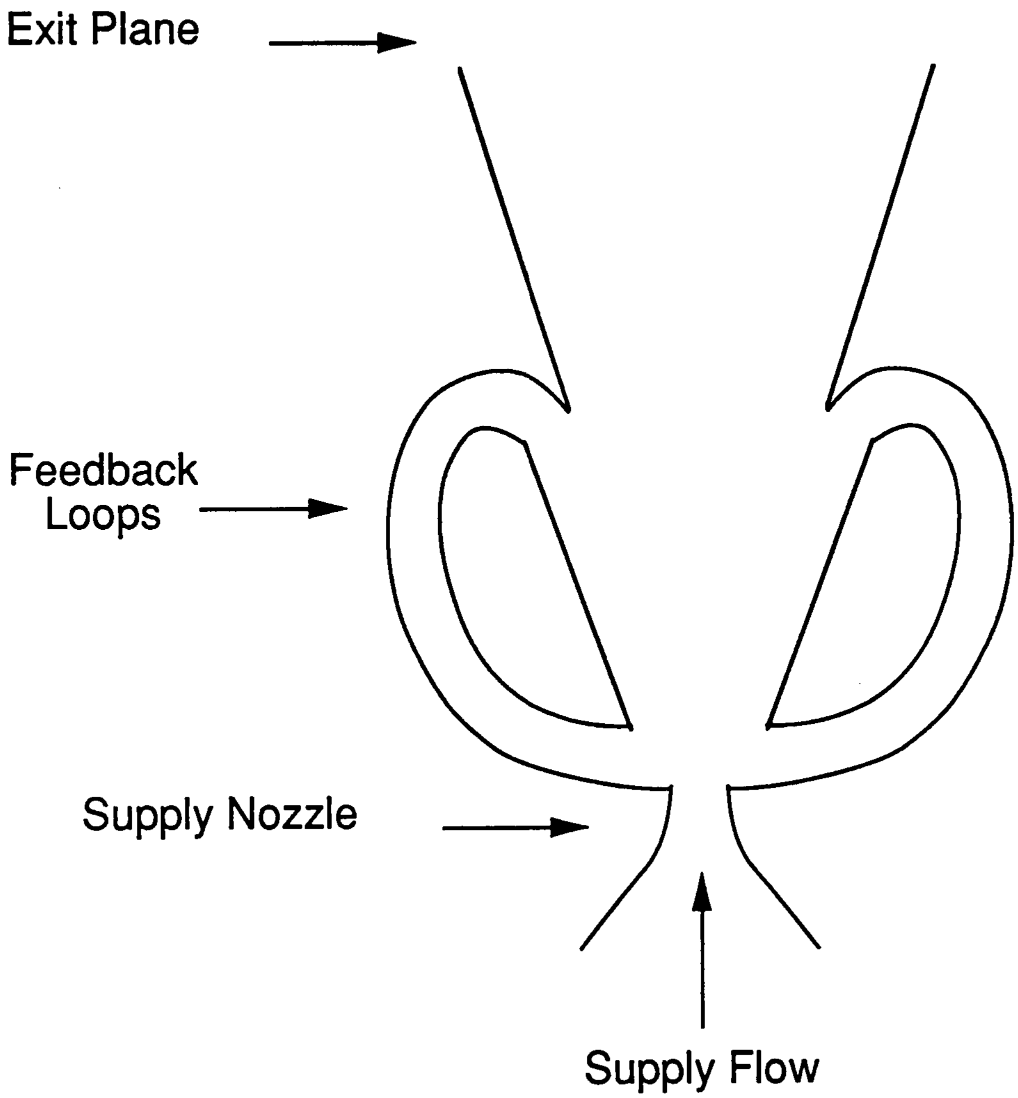

Figure 2.3. Fluidic Oscillator.

by S. M. Riddlebaugh[3], using various gases, demonstrates a similar relationship whereby pressure drop is proportional to frequency of oscillation until a choked nozzle condition is established. Under choked flow conditions, frequency becomes pressure independent.

Wall Attachment Theory

The fundamentals of wall attachment theory can be applied to fluidic oscillators. Since the feedback loops transmit some of the main flow to the control, the control flow is merely a function of the supply flow. A number of simplified models have attempted to relate the geometrical and fluid parameters to the jet attachment point and the separation bubble pressure[5]. Most analyses assume that the jet centerline moves like that of a circular arc commencing at the center of the orifice and terminating at the wall attachment point. Good agreement with empirical data has, also, been achieved assuming a sinusoidal curve for the jet path. The actual shape of the jet path is not completely understood and serves to distinguish different theoretical approaches in the design of fluidics. This study makes the circular arc assumption.

The designs of most fluidic devices are either planar (two-dimensional) or axisymmetric. In most two-dimensional fluidic devices, the aspect ratio, defined as the ratio of the channel height to the nozzle width, is small because of the need for low power consumption, miniaturization and low noise. Dohta et. al.[6] have examined the effects of aspect ratio on the static behavior and switching of an attaching jet. The results indicate that for large control flow rates, there is a remarkable increase in attachment distance when the aspect ratio is increased. It is suggested that due to the longer distance, the influence of the boundary layer on the bounding plates becomes dominate and an increased control rate is required. For a decreasing aspect ratio, it follows that a decreased amount of switching control flow is needed. In devices of small aspect ratio, however, the jet flow cannot always be regarded as two-dimensional due to the existing boundary layer on the top and bottom plates and the secondary flow resulting from a bounding jet. A value of two for aspect ratio has generally been used as an acceptable value and is the value used in this analysis.

Kirshner and Katz[7] present measurements of the velocity profile that indicate, even near the point of attachment, each half of the jet has almost the same half profile shape as that of a free jet. The spread factor (σ_e), which is defined so that increased spreading is reflected in a reduction of the spread factor, is different, however, for the attached side of the jet compared to the unattached side of the jet. Examination of the spreading of two-dimensional jets indicate that bounded jets spread less than a free jet. The decrease in spreading is due to the restriction of the lateral entrainment flow caused by the friction on the bounding plates. Increasing the area of the top and bottom plate increases the resistance and causes the jet to spread even less. Furthermore, the spread factor is largest near the nozzle and reduces asymptotically to a constant value (approx. $\sigma_e = 10$). Most theoretical analyses, however, tend to use a constant spread factor in the design analysis. Kinoshita and Murakimi[8] in their study of the effects of curved walls in the design of fluidic devices use a value of $\sigma_e = 7.2$. Romiti[9] states that for small slopes and offsets, a value of $\sigma_e = 6$ is more suitable. The free jet approximation, $\sigma_e = 7.67$, is normally used for straight wall devices and is the value used in this study.

Governing Equations

The following derivation of governing equations follows that developed by Kirshner and Katz[7]. Consider the two dimensional, inviscid, incompressible flow case of jet attachment as it pertains to the device illustrated in Figure 2.4(a). The supply flow, (q_{sup}), emerges from a nozzle of width b and attaches to a straight wall inclined at an angle α. The wall is off-set from the nozzle at a distance B. The control flow, (q_c), is applied from the feedback loops of width b. Figure 2.4(a), also, shows the mean resultant streamlines. The entrainment streamline, (I), is forced away from the wall by the control flow. The attachment streamline, (II), is projected from one side of the control nozzle to the attachment point. Since the flow does not cross a streamline, the flow between streamlines I and II is q_c. By examining the attached-side velocity profile in Figure 2.4(b), the flow between y_E and y_∞ can be defined as the entrained flow (q_e), whereas, the flow between y_A and y_∞ is the return flow (q_r). Thus, q_c is, merely, the difference between the two flows;

$$q_c = q_e - q_r$$

In order to obtain a relationship between q_c and q_{sup}, the following equation must be solved;

$$\frac{q_c}{q_{sup}} = \frac{q_e}{q_{sup}} - \frac{q_r}{q_{sup}} \tag{1}$$

From the velocity profile in Figure 2.4(b), which represents only half the entire velocity profile, q_e can be defined as follows;

$$q_e = h \int_0^\infty u(s, y) dy - \frac{q_{sup}}{2} \tag{2}$$

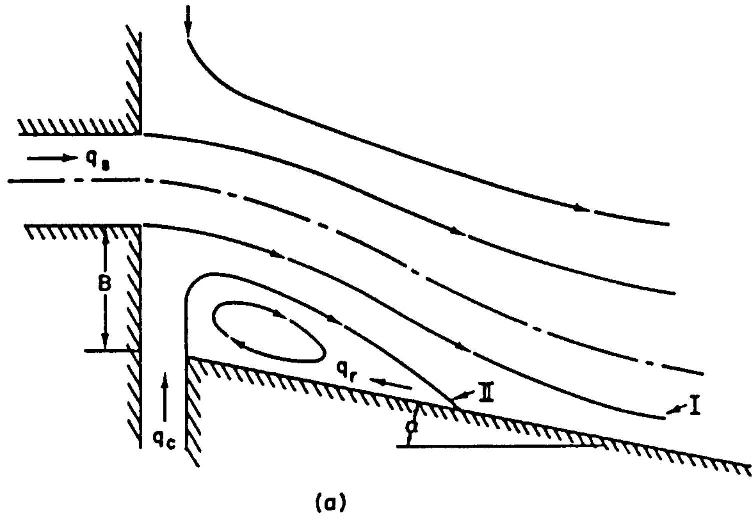

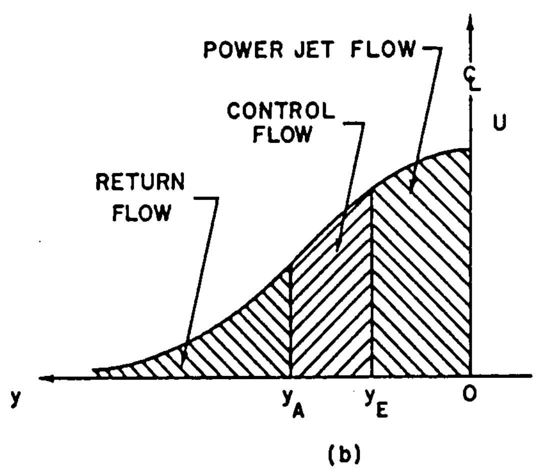

Figure 2.4. Jet Attachment With Control Flow: (a) Mean Flow Streamlines, (b) Attached-Side Velocity Profile. (From Kirshner and Katz[6])

where h is the depth of the nozzle and $u(s, y)$ is the fluid velocity at a given point on a streamline, (s), and a perpendicular distance away from the streamline, (y). Similarly, q_r is defined as;

$$q_r = h \int_{y_A}^{\infty} u(s, y) dy \tag{3}$$

Approximating the jet velocity profile and applying the inviscid flow assumptions, the wall friction forces are neglected. The velocity profile model used in this analysis is that developed by Bourque and Newman[10]. It is a modified Goertler profile[7] for a turbulent two dimensional free jet as follows;

$$u(s, y) = k_3 \text{sech}^2(k_4 y) \tag{4}$$

where;

$$k_3(s) = \frac{1}{2} \left[\frac{3 J \sigma_e}{\rho(s + s_0)} \right]^{\frac{1}{2}}$$

$$k_4(s) = \frac{\sigma_e}{(s + s_0)}$$

and $J = \rho u^2 b$, the momentum flux out of the nozzle per unit depth.

The origin of the flow is assumed a distance, s_0, upstream of the nozzle exit plane so that q_{sup} can be estimated by a free jet. Referring to the illustration in

Figure 2.5, the constant, s_0, can be calculated by projecting the velocity profile to the supply nozzle exit plane ($s = 0$), such that the entire velocity distribution is due to q_{sup} only. Therefore, the velocity profile can be integrated to find q_{sup} at $s = 0$ as follows;

$$q_{sup} = 2h \int_0^\infty u(s, y)dy$$

$$= 2h \int_0^\infty k_3(0)\text{sech}^2(k_4(0)y)dy$$

$$= 2h \frac{k_3(0)}{k_4(0)}$$

Hence;

$$q_{sup} = h \left(\frac{3Js_0}{\rho \sigma_e} \right)^{\frac{1}{2}} \tag{5}$$

Using the modified Goertler profile at the point $s = s_0$, the same result is obtained. However, the point s_0 is inside the channel and such a volume flow due to a uniform flow distribution can be simply expressed as the product of the flow velocity and the channel cross sectional area. Thus;

$$q_{sup} = u_0 bh \tag{6}$$

By equating equations (5) and (6);

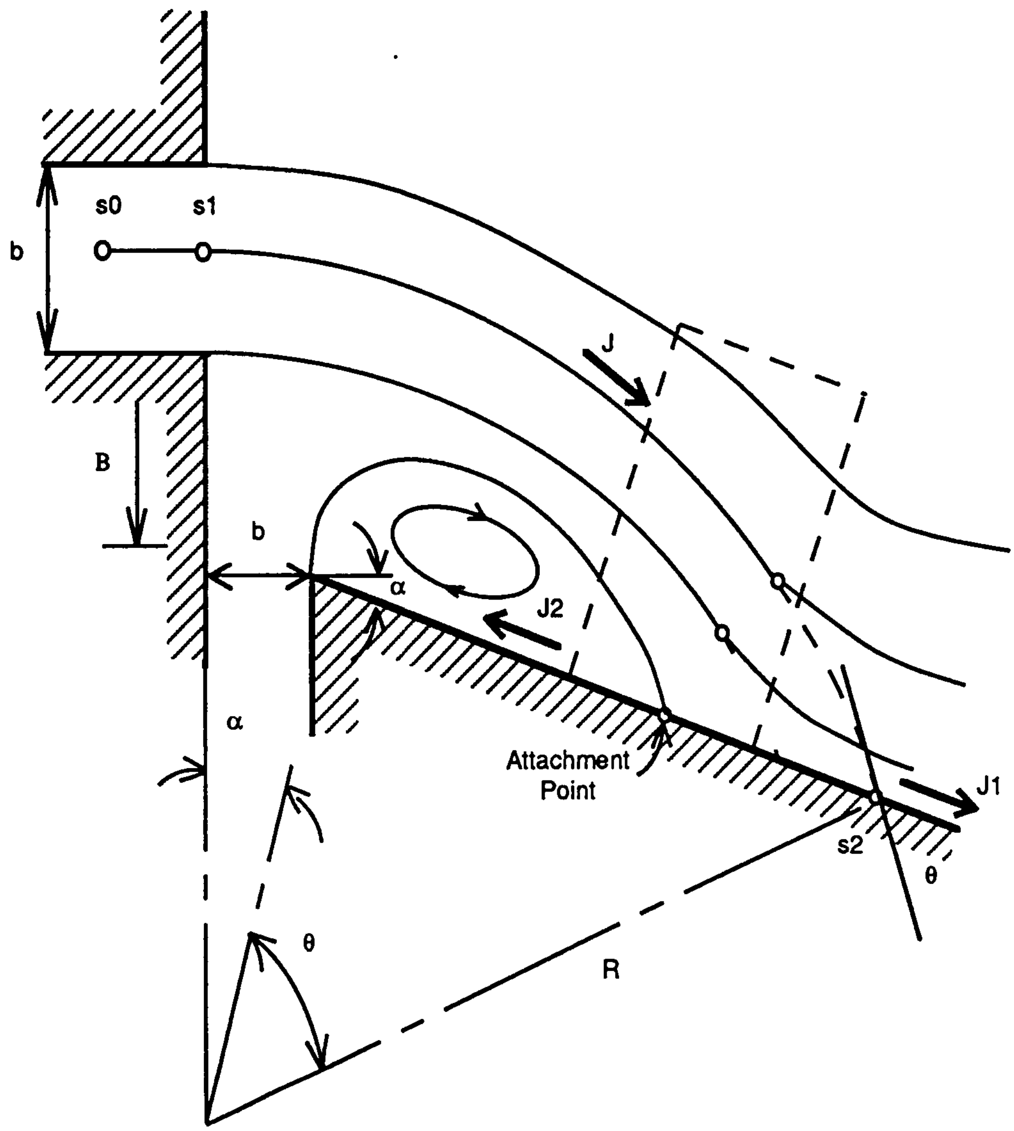

Figure 2.5. Jet Attachment To An Offset Inclined Wall With Control Orifice.

$$u_0 bh = h\left(\frac{3Js_0}{\rho\sigma_e}\right)^{\frac{1}{2}}$$

Recall $J = \rho u^2 b$,the momentum flux out of the nozzle per unit depth. Hence, solving for s_0;

$$s_0 = \frac{\sigma_e b}{3} \tag{7}$$

Substituting this back into equation (4), the final form of the velocity profile is given as;

$$u(s,y) = \frac{1}{2}\left[\frac{3J\sigma_e}{\rho(s+\frac{\sigma_e b}{3})}\right]^{\frac{1}{2}} \operatorname{sech}^2\left(\frac{y\sigma_e}{s+\frac{\sigma_e b}{3}}\right) \tag{8}$$

As can be seen from Figure 2.5, the extension of the circular arc made by the jet center line occurs when $s = s_2$. Substituting equations (5) and (8) into equation (2) for $s = s_2$, the following is found;

$$\frac{q_e}{q_{sup}} = \int_0^{\infty} \frac{1}{2}\left[\frac{3\sigma_e}{b(s_2+\frac{b\sigma_e}{3})}\right]^{\frac{1}{2}} \operatorname{sech}^2\left(\frac{y\sigma_e}{s_2+\frac{b\sigma_e}{3}}\right) dy - \frac{1}{2}$$

To integrate use the relation, $\int \operatorname{sech}^2(ax)dx = \frac{\tanh(ax)}{a}$. Thus;

$$\frac{q_e}{q_{sup}} = \frac{1}{2}\left[\left[\frac{s_2+\frac{b\sigma_e}{3}}{\frac{b\sigma_e}{3}}\right]^{\frac{1}{2}} - 1\right] \tag{9}$$

The same integration process can be applied to equation (3) to get the following result for the return flow;

$$\frac{q_r}{q_{sup}} = \frac{1}{2}\left[\frac{s_2 + \frac{b\sigma_e}{3}}{\frac{b\sigma_e}{3}}\right]^{\frac{1}{2}}\left[1 - \tanh\left(\frac{\sigma_e y_A}{s_2 + \frac{b\sigma_e}{3}}\right)\right] \tag{10}$$

Finally, by substituting in equations (9) and (10) into equation (1), the equation of the attachment streamline can be found as follows;

$$\frac{q_c}{q_{sup}} = \frac{1}{2}\left[\left[\frac{s_2 + \frac{b\sigma_e}{3}}{\frac{b\sigma_e}{3}}\right]^{\frac{1}{2}} \tanh\left(\frac{\sigma_e y_A}{s_2 + \frac{b\sigma_e}{3}}\right) - 1\right] \tag{11}$$

Equation (11) cannot be solved explicitly as there are too many unknowns. Another equation comes from examining the momentum flux surrounding the attachment point. Applying Bourque and Newman's[10] approach, assume that the momentum flux is conserved in a volume surrounding the attachment point. Neglecting the effects of pressure, the average angle of the input momentum flux, J, is essentially the same angle made if the centerline were extended (refer to Figure 2.5). Thus,

$$J\cos(\theta + \alpha) = J_1 - J_2$$

where;

$J_1 = \rho \int_{-\infty}^{y_A} u^2 dy$

$J_2 = \rho \int_{y_A}^{\infty} u^2 dy$

J_1 and J_2 can be calculated using equation (4). The resulting equation is;

$$\cos(\theta + \alpha) = \frac{3}{2}\left[\tanh\left(\frac{\sigma_e y_A}{s_2 + \frac{b\sigma_e}{3}}\right) - \frac{1}{3}\tanh^3\left(\frac{\sigma_e y_A}{s_2 + \frac{b\sigma_e}{3}}\right)\right] \tag{12}$$

Three further equations can be found through geometrical considerations. By assuming the jet moves with a constant radius of curvature, it can be seen from Figure 2.5 that the following relationships exist;

$$R\left(1 - \frac{\cos\theta}{\cos\alpha}\right) = B + \frac{b}{2} \tag{13}$$

$$R(\alpha + \theta) = s_2 \tag{14}$$

$$x_R + \frac{y_A}{\sin\theta} = R(\sin\theta + \cos\theta\sin\alpha) \tag{15}$$

where, x_R is the distance along the wall to the attachment point.

To determine the attachment distance, the values of B, b, α, σ_e, and $\frac{q_c}{q_{sup}}$ must be specified leaving the desired 5 equations with 5 unknowns. The unknowns are the geometrical constraints, θ, y_A, x_R, s_2, and R. In order to solve for attachment distance as a function of $\frac{q_c}{q_{sup}}$, equations (11)-(15) were algebraically manipulated down to two equations with two unknowns; θ and x_R. Since θ had to be solved implicitly, a Newton Raphson iteration technique was employed. The computer program enclosed as Appendix A was constructed to solve for $\alpha = 12^o$ and $\sigma_e = 7.67$ for a range of $\frac{q_c}{q_{sup}}$. Refer to Figure 2.6 for the effect of the control flow on attachment distance.

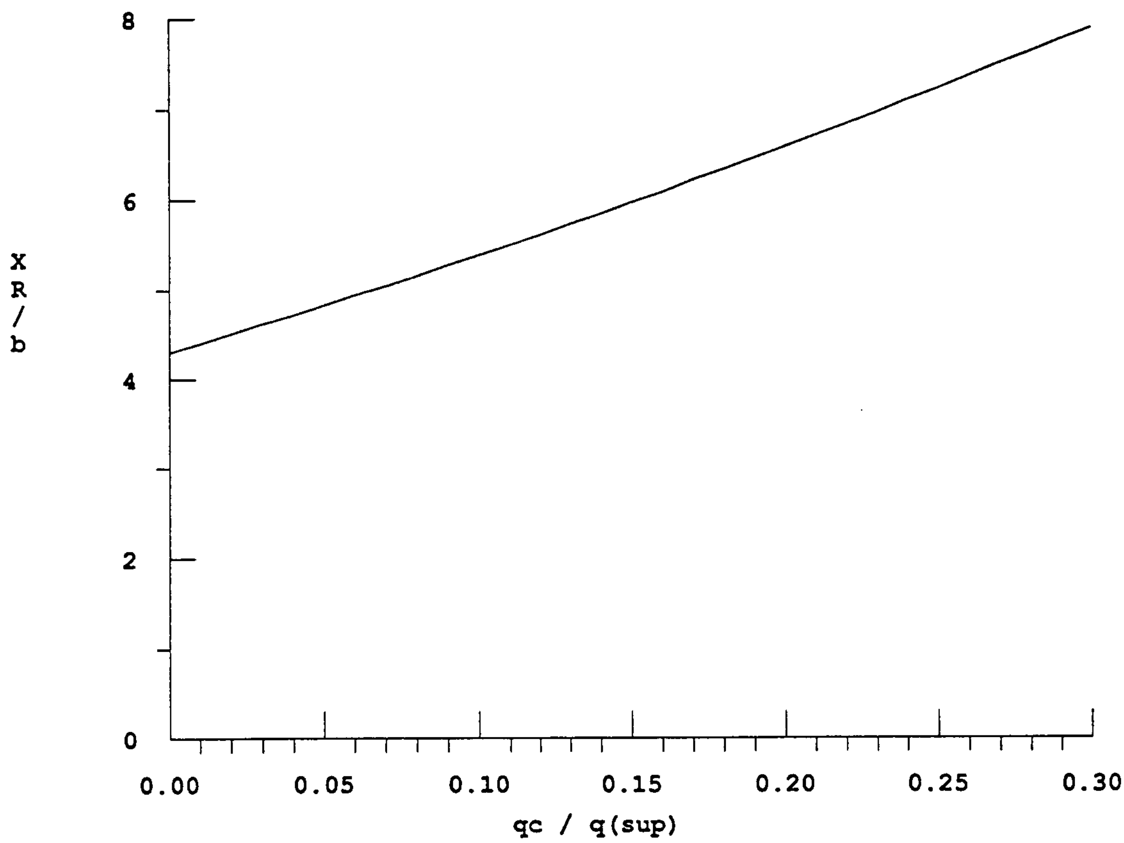

Figure 2.6. Effect Of Control Flow On Jet Attachment Distance For $\alpha = 12^o$ and $\sigma_e = 7.67$.

Understandably, the results obtained using wall attachment theory cannot be directly applied in the design of every fluidic device. The geometry of the devices will, for most part, dictate the suitability of application. Especially for fluid oscillators, where the actual value of $\frac{q_c}{q_{sup}}$ is not defined. In this study, the results obtained from wall attachment theory for a range of $\frac{q_c}{q_{sup}}$ were considered as being somewhat conservative and the attachment distance used for the design of the fluidic oscillator was twice that predicted by the maximum value of $\frac{q_c}{q_{sup}}$ calculated.

CHAPTER III

QUALITATIVE ANALYSIS

Experimental Method

This phase of the experiment was carried out in the water tunnel. A plexiglas model was constructed, the design of which was based upon results of wall attachment theory. Refer to Appendix B for the design specifications of the plexiglas model. Several configurations were tested and analyzed. Figure 3.1 shows the different variations examined.

A schematic illustration of the experimental set-up is provided in Figure 3.2. Throughout the experimental procedure, the model was submerged in the water tunnel and fixed in place. This allowed for flow visualization and eliminated voids and bubbles in the system. A flexible water hose was connected to the input of the device to provide the supply flow. The input flow rate was measured using a flow meter. Flow visualization was performed by injecting dye into ports on the model surface. The locations of the dye ports are shown in Figure 3.2. The dye was made from a mixture of food coloring, milk and alcohol to achieve the desired specific gravity of one. The water tunnel was run at a speed sufficient to carry the dye downstream of the test section so that it would not obstruct the visualization technique.

Water Tunnel Results

When the initial configuration, shown in Figure 3.1(a), was tested, the fluidic device did not function as an oscillator as expected. Based upon the analysis of the flow visualization, it was determined that the wall attachment point was

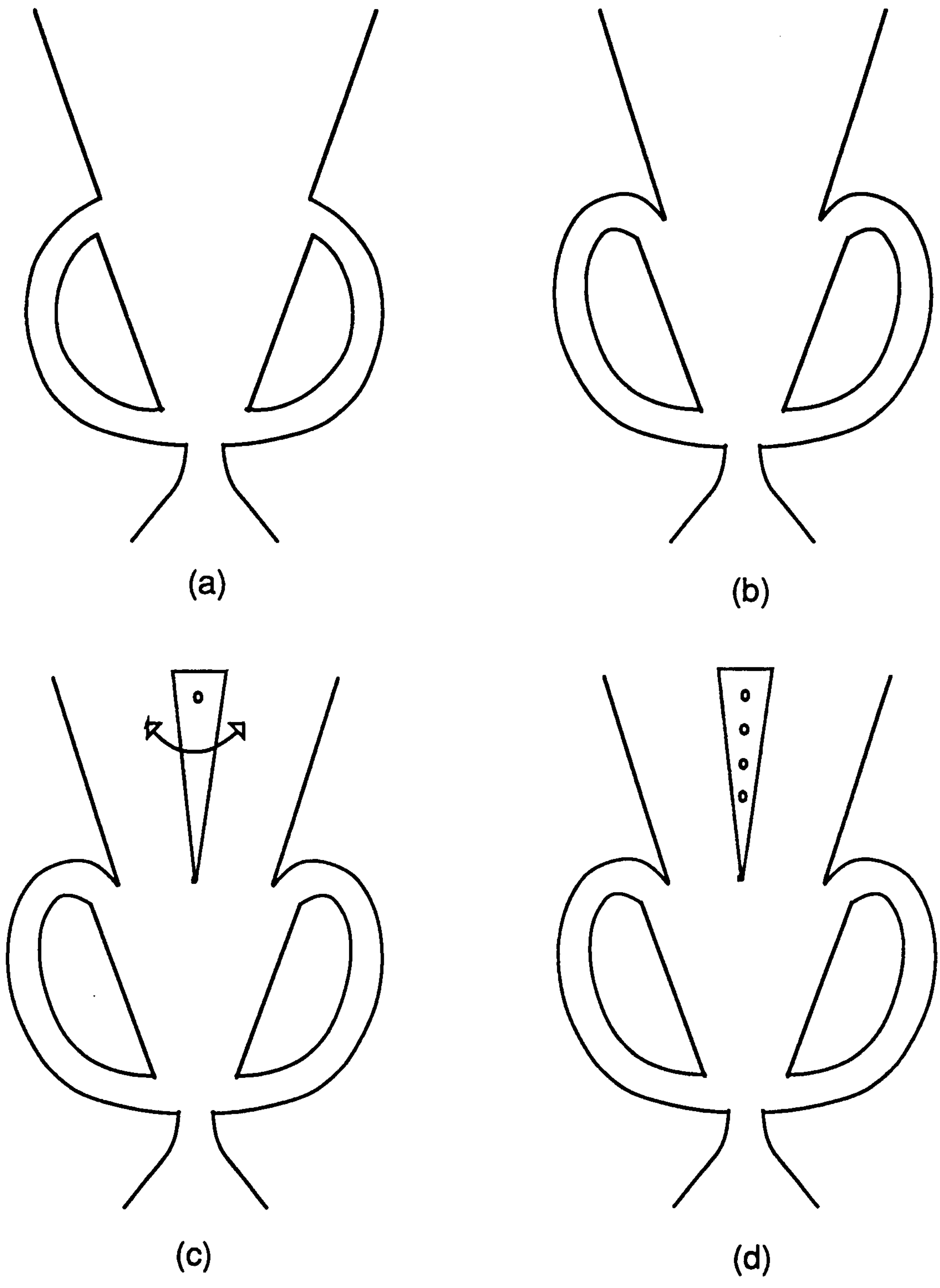

Figure 3.1. Plexiglas Model Configurations : (a) Initial Configuration, (b) Modified Feedback Loop Entrance, (c) Wedge With One Degree Of Freedom, (d) Fixed Wedge.

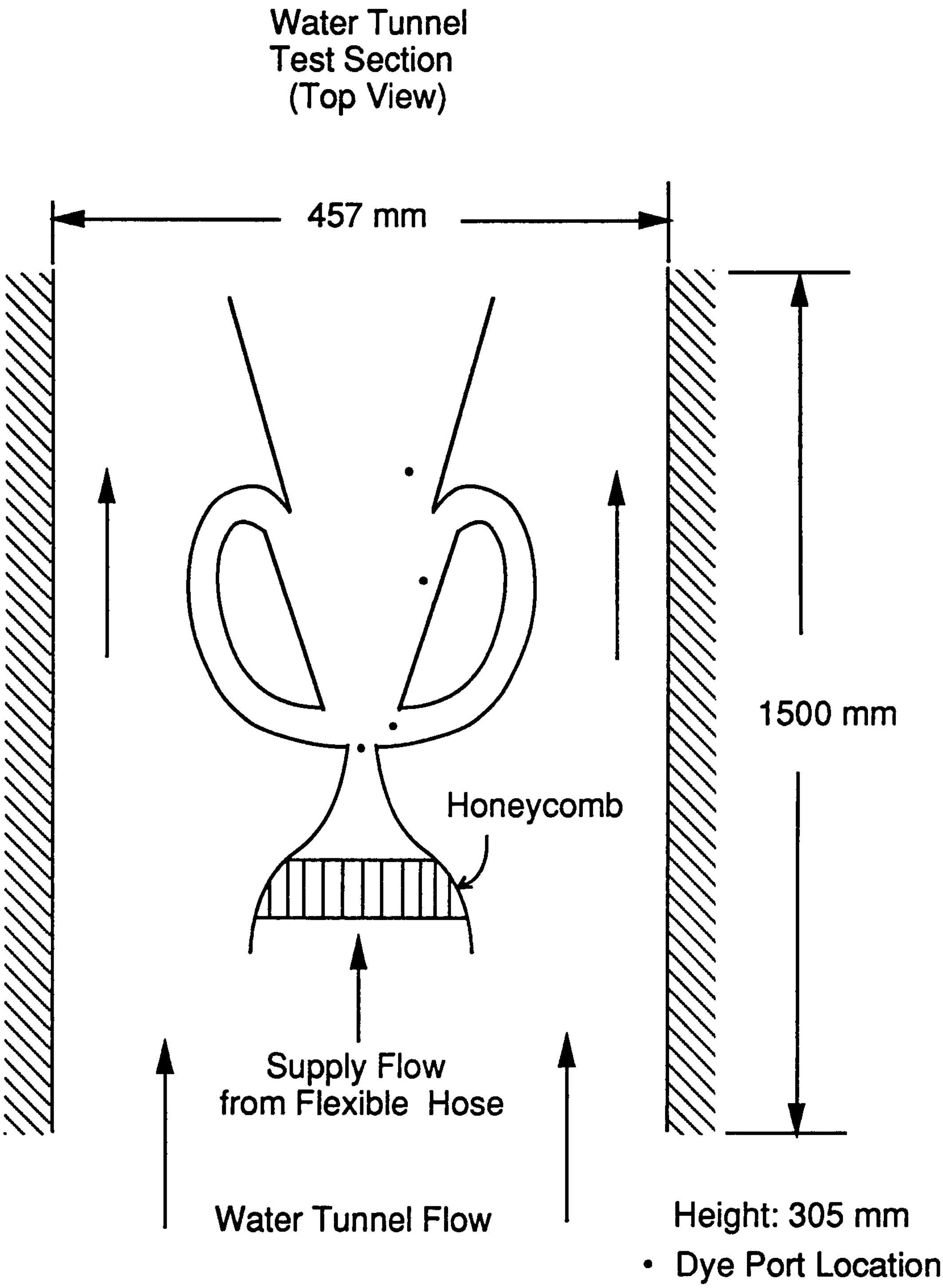

Figure 3.2. Experimental Set-Up Of Water Tunnel.

occurring well before the entrance to the feedback loop and, as such, the pressure pulse that was provided through the loop and felt in the separation bubble was not strong enough to cause switching of the jet. Since it is known that wall attachment distance increases with increased supply flow rate, it would have been possible to increase the supply flow rate until such a point that wall attachment occurred precisely at the entrance to the feedback loop and perhaps the momentum of the attaching flow may have been sufficient to sustain oscillation. However, since the supply of water was restricted, the model configuration was modified.

The modification made to the model was designed to take advantage of the momentum of the supply flow regardless of where wall attachment occurred. If, however, it was required that the fluidic oscillator have frequency optimized, it would have been essential that the wall attachment point be made to occur at the entrance to the feedback loops. The design of the entrance to the feedback loops as shown in Figure 3.1(b) does ensure flow oscillation for all supply flow rates. Visualization of the continuous flow process clearly illustrated the oscillatory behavior of the fluidic device. Referring to the photograph in Figure 3.3(a), the dye emanating from the supply nozzle shows the flow attached to the upper side wall. This photograph, also, shows dye emanating from the center of the lower wall which is following the flow downstream and getting trapped by the entrance of the lower feedback loop. In the photograph of Figure 3.3(b) the dye coming from the supply nozzle shows the flow in the process of switching sides. The dye coming from the center of the lower wall now illustrates a reverse flow along the wall as well as the forming of a separation bubble. The dye that was previously trapped by the entrance to the feedback loop is now shown as it is being forced through the feedback loop. It is this pulse of fluid that increases the pressure in the separation bubble and causes jet switching. By introducing dye into various combinations of

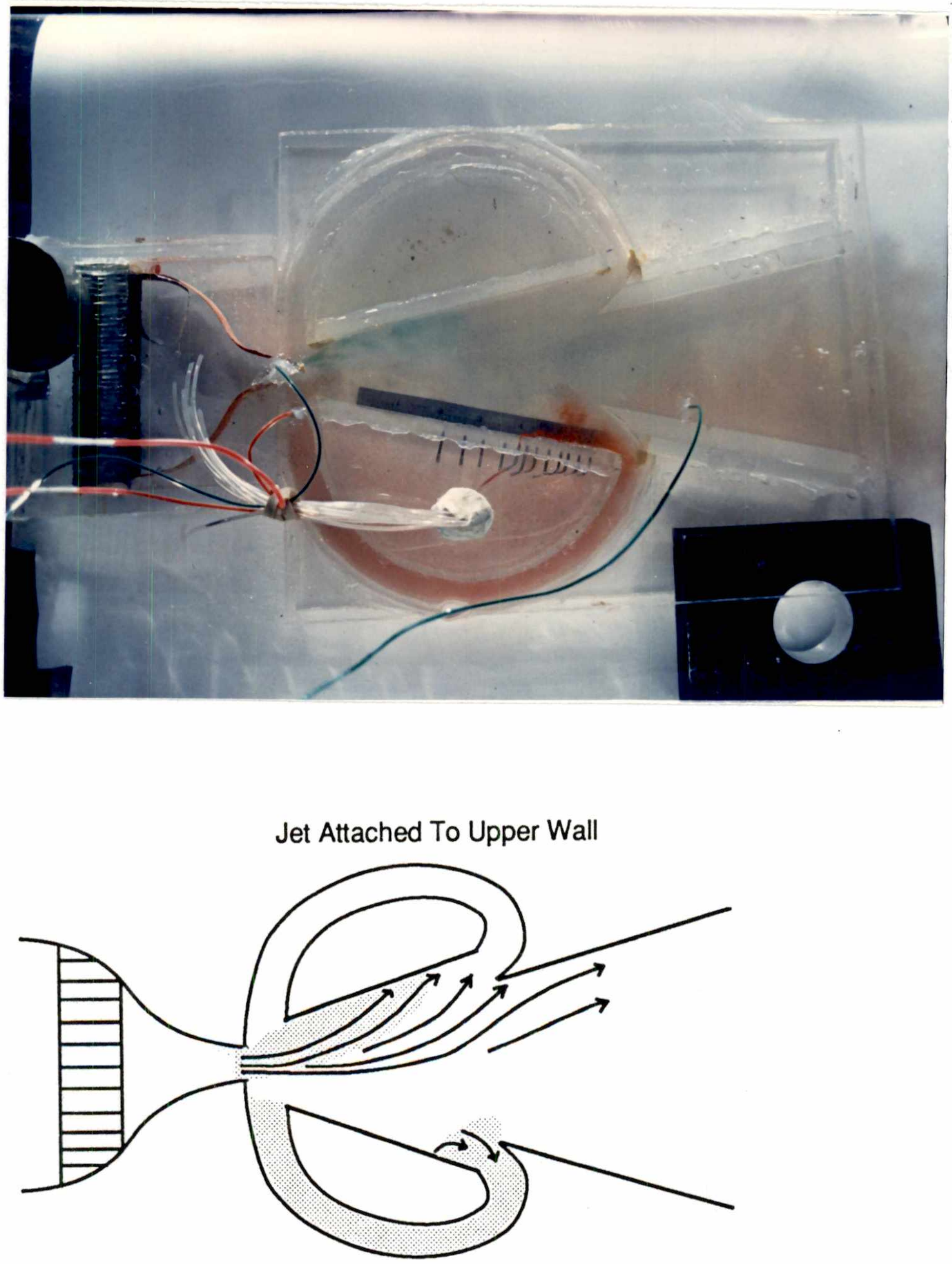

(a) Jet Attached To Upper Wall

Figure 3.3. Flow Visualization Of Configuration In Figure 3.1(b): (a) Jet Attached To Upper Wall; (b) Jet Attached To The Opposite Side.

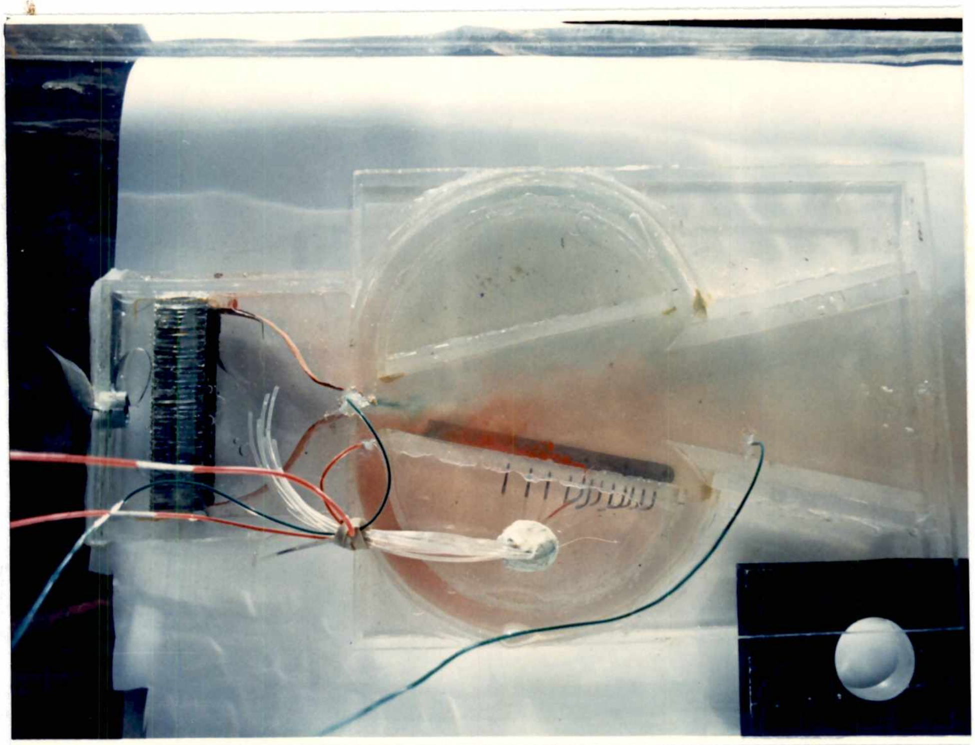

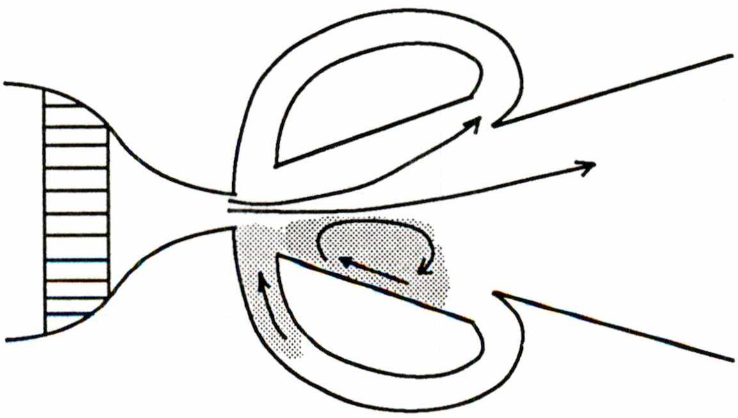

Fluid Pulse Through The Lower feedback Loop.
Reverse Flow On Lower Wall.
Forming Of Separation Bubble.

(b) Jet Attached To The Opposite Side

Figure 3.3. (Continued)

the other dye ports, it was possible to see the entire switching phenomenon. It was very interesting to note that the output of the flow appeared to occur entirely on one side of the exit plane while the other side of the exit plane demonstrated a reverse flow or suction. This phenomenon lent credibility to the application of the fluidic oscillator as a device to provide a distinct pulsed output.

The configuration, shown in Figure 3.1(c), was devised to achieve an assessment of the frequency of oscillation. The wedge was, only, held in place by one pin thus allowing it a single degree of freedom. The frequency of oscillation was calculated by counting the number of times the wedge returned to its original position in a fixed period of time. A plot of frequency verses supply flow rate is provided in Figure 3.4. An approximately linear relationship is shown to exist between frequency and supply flow rate. A similar linear relationship was found in the experiments on fluidic oscillators performed by Beale and Lawler[3]. The slight nonlinearity of this study's results can be attributed to minor leaks of the bonding material in the model structure and to the inaccurate method of the model's construction. The photograph in Figure 3.5, demonstrates a benefit of having a moving part. While the wedge is attached to one side it is able to completely close the flow on one side of the output while allowing for the entire flow output through the other side.

The final configuration that was tested is shown in Figure 3.1(d). A rigid splitter wedge was located along the axis of symmetry. The position of its apex was varied from being close to the supply nozzle to being at the model exit. Test runs were carried out to determine whether or not installing a flow separating device in the design of the fluidic oscillator would influence the flow behavior. Through the flow visualization technique, it was found that when the wedge apex was situated by the entrance to the feedback loops and further downstream toward the exit

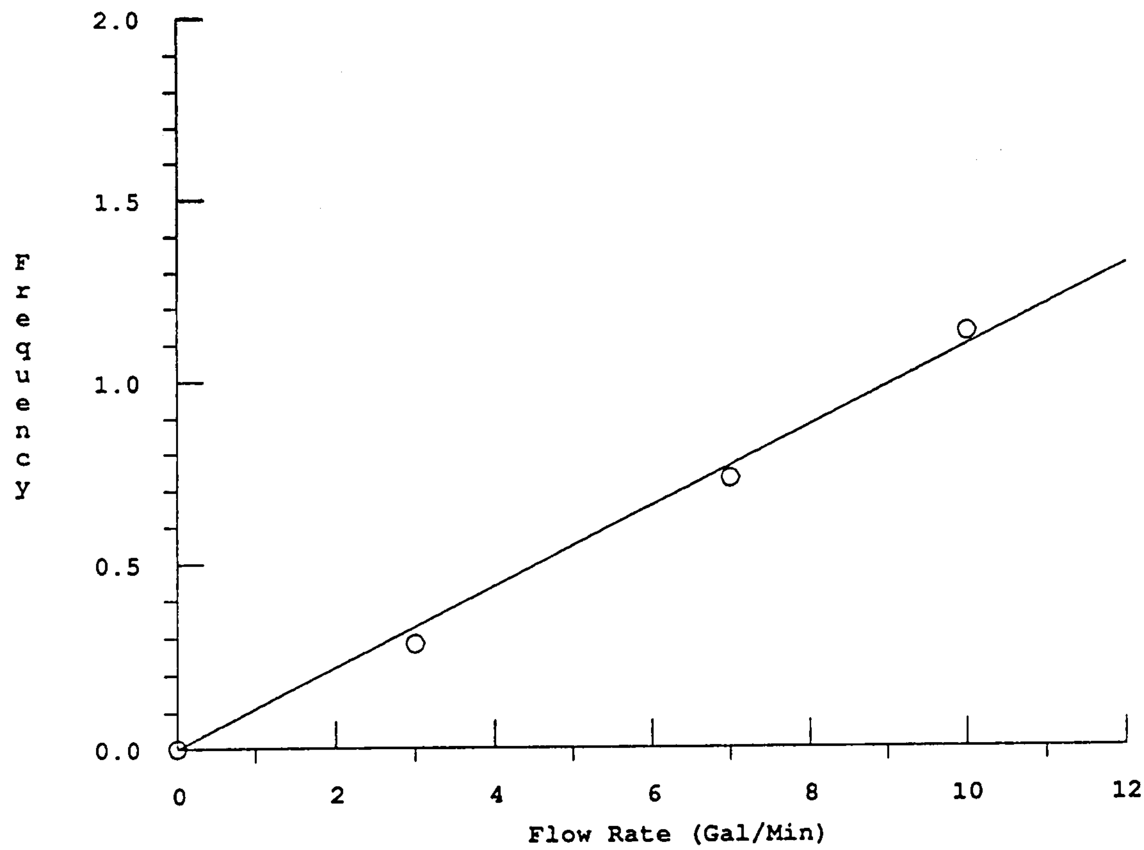

Figure 3.4. Relationship Between Frequency And Supply Flow Rate.

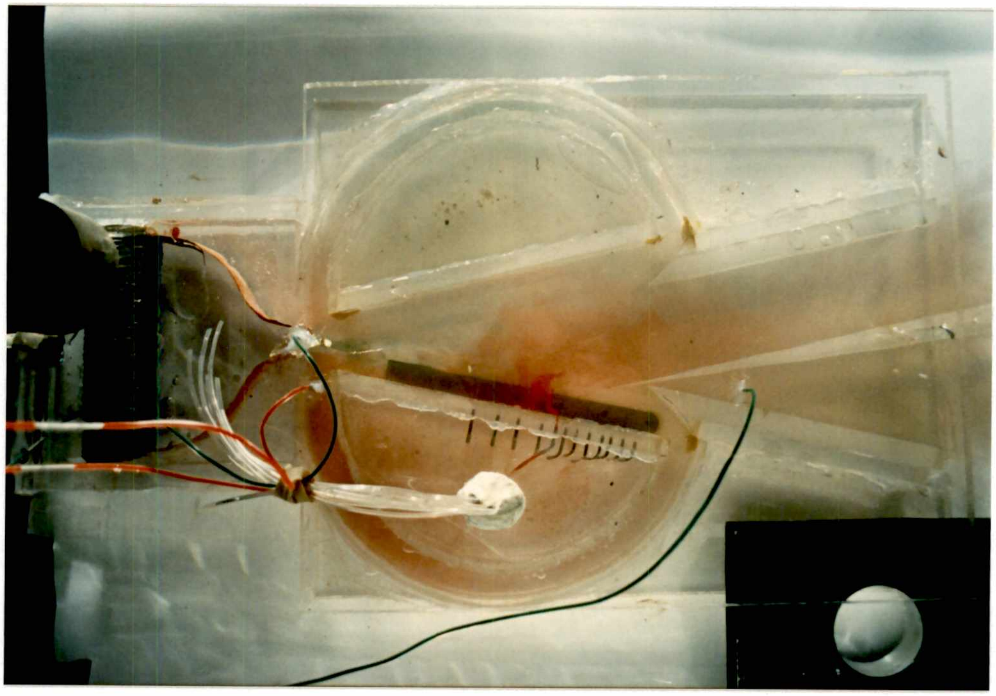

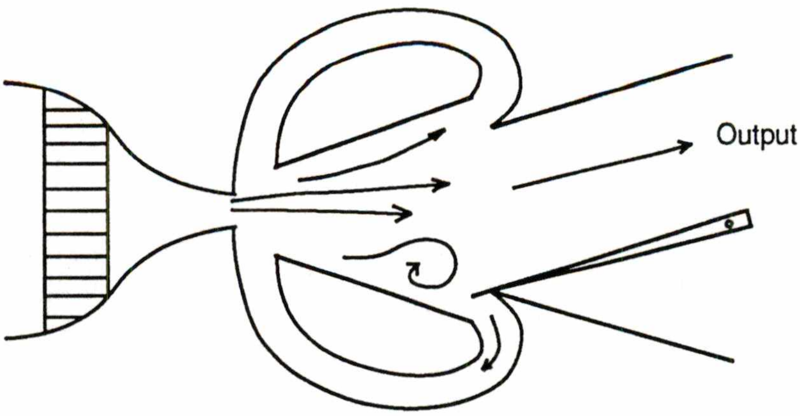

Figure 3.5. Flow Visualization Of Configuration In Figure 3.1 (c) : Wedge Completely Closes One Side Of Output Resulting In Distinct Pulse Through The Other Side.

plane, the oscillatory behavior of the fluidic device was not noticeably affected. In fact, as shown in the photograph of Figure 3.6, a distinct pulse of fluid flow is being forced through one side of the output while the other side remains clear. As the apex of the wedge was moved closer to the supply nozzle, however, the influence of the wedge became more profound and eventually caused the oscillatory behavior to cease.

Conclusions

The results of the water tunnel experiment were encouraging. The linear relationship found between frequency and flow rate added credibility to the design specifications. The plexiglas model, however, could not be used to acquire accurate quantitative results. The model was not built to very small tolerances and there were leaks in the bonding material. A new model, machined to precision, was therefore constructed out of aluminum. Since it was found that placing a wedge in the flow field had an influence in the flow's behavior, which merely complicated the flow, the wedge was not included in the new design. The design specifications of the aluminum model were the same as the plexiglas model (enclosed as Appendix B). The purpose of building the new model was to get an accurate assessment of frequency of oscillation and to gain a better understanding of the output characteristics.

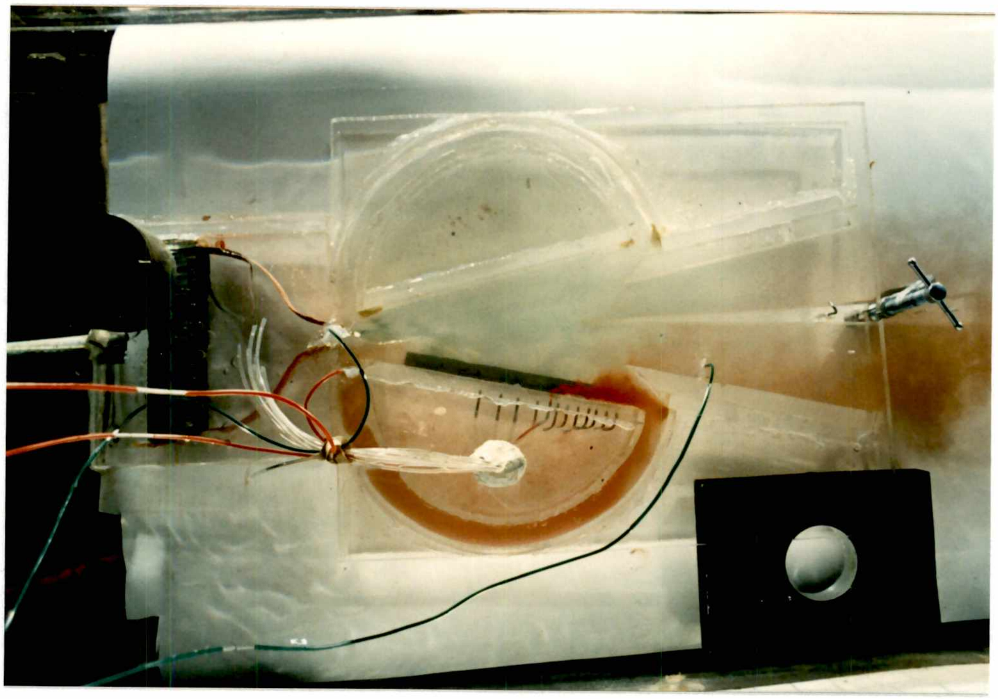

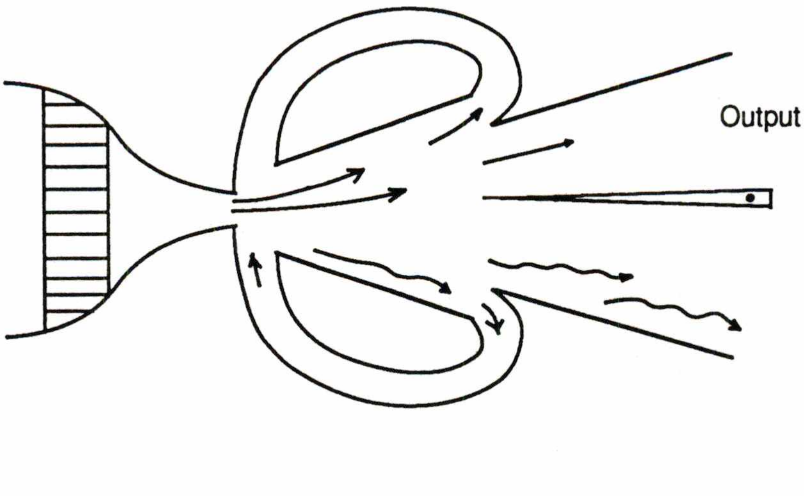

Figure 3.6. Flow Visualization Of Configuration In Figure 3.1(d) Shows A Pulse Of Fluid Flow Through One Side While The Other Side Remains Clear.

CHAPTER IV

QUANTITATIVE ANALYSIS

Test Program

In this final portion of research, an aluminum model was tested with air as the medium. The photograph in Figure 4.1 provides an illustration of the model that was tested. The top of the model was made out of a removable piece of plexiglas. This allowed for flow visualization and facilitated easy access to the model's interior. A large number of bolts were used in attaching the plexiglas top to the model to ensure its structural integrity and rubber o-rings were employed around the entire perimeter of the device to ensure its air-tight nature. To assist in providing a smooth flow to the supply nozzle, two segments of honey-comb were installed in the center region of the stilling chamber. The model itself was rigidly connected to a heavy metal stand to minimize vibrations. Air was supplied to the model by two inch diameter low pressure hose. The photograph in Figure 4.2 illustrates the overall experimental set-up.

The placement of instrumentation used for data collection is outlined in Figure 4.3. A total pressure probe was located in the distilling chamber and a static pressure port was situated in the nozzle throat. Through simple application of compressible flow relations, the nozzle throat velocity was calculated. In the entrance of one of the feedback loops, a dynamic pressure probe was mounted flush to the model floor. A Spectrum Analyzer was linked to the output of the dynamic pressure probe so that the frequency of oscillation was monitored. At the exit plane of the model, a traversing mechanism was incorporated that allowed a total pressure probe to be moved across the exit plane.

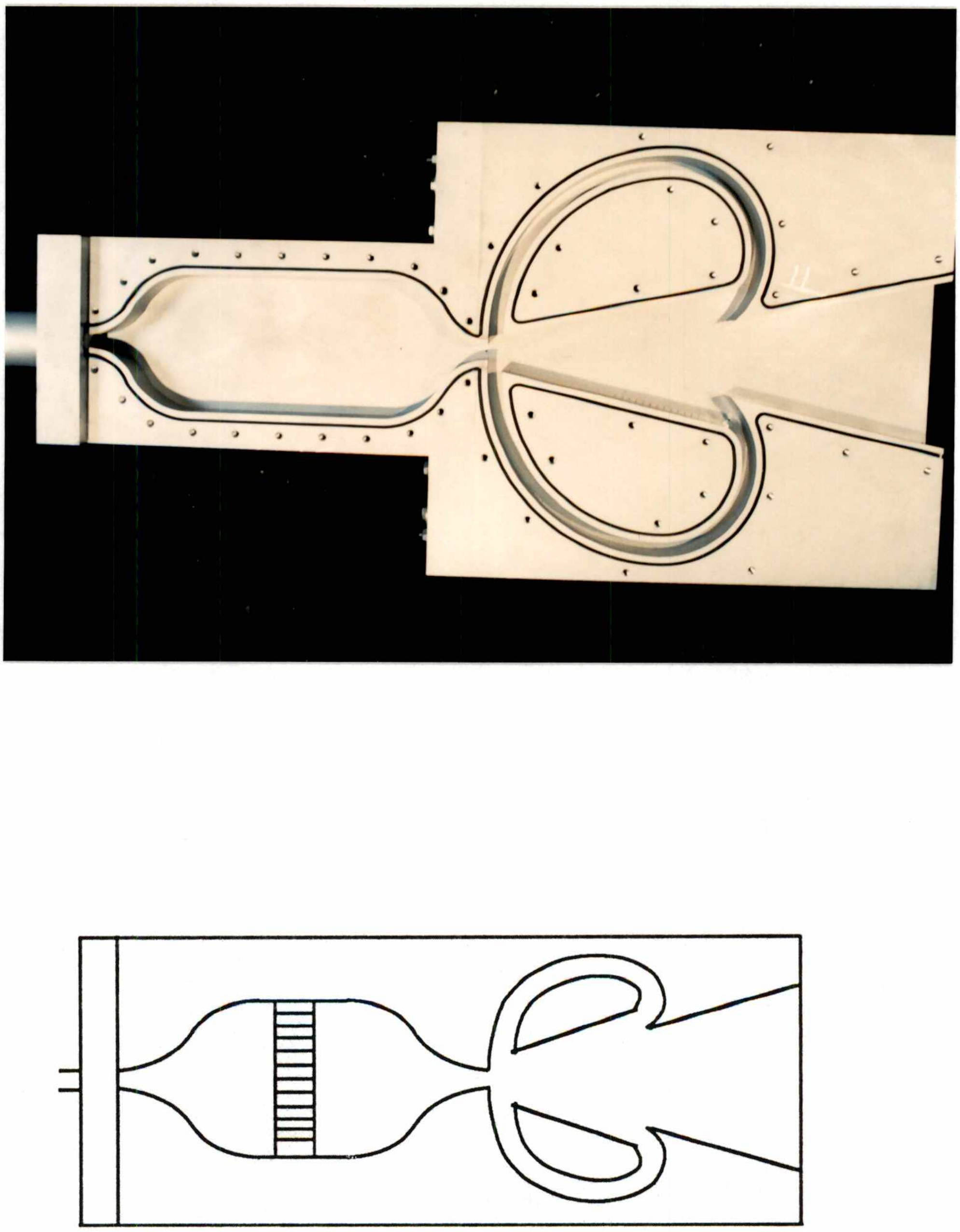

Figure 4.1. Aluminum Test Model.

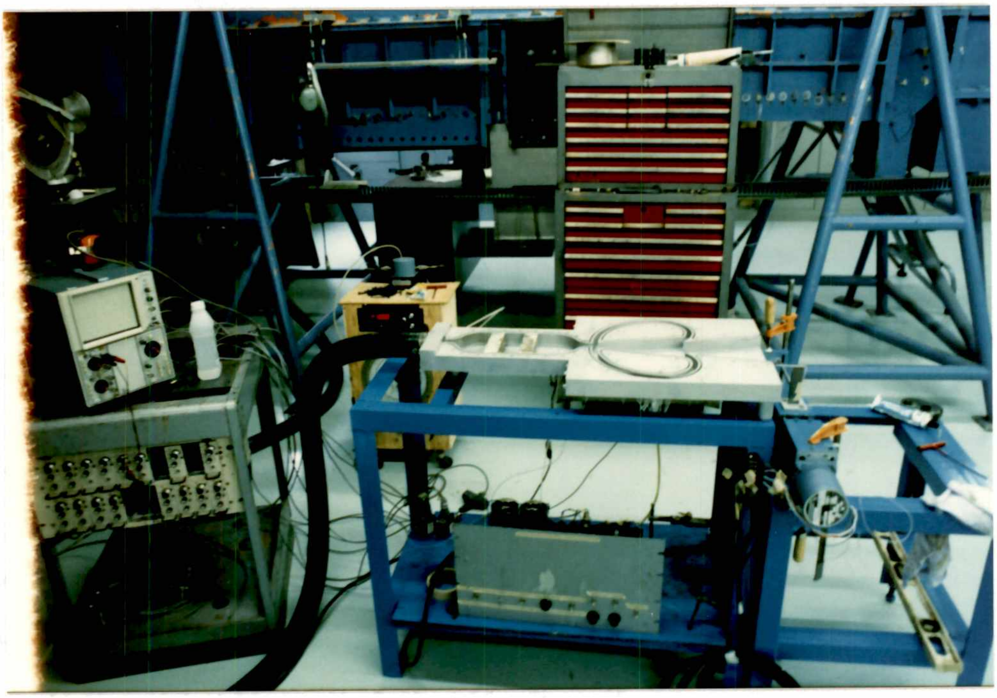

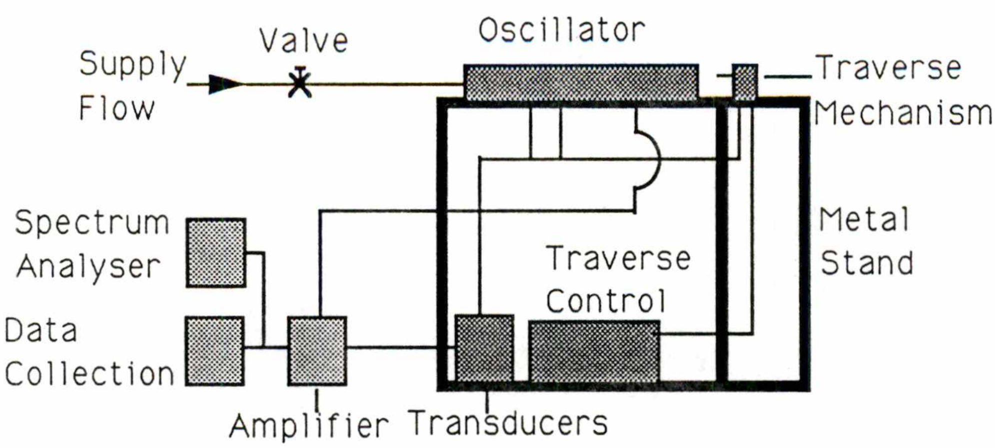

Figure 4.2. Experimental Set-Up Of Air Tests.

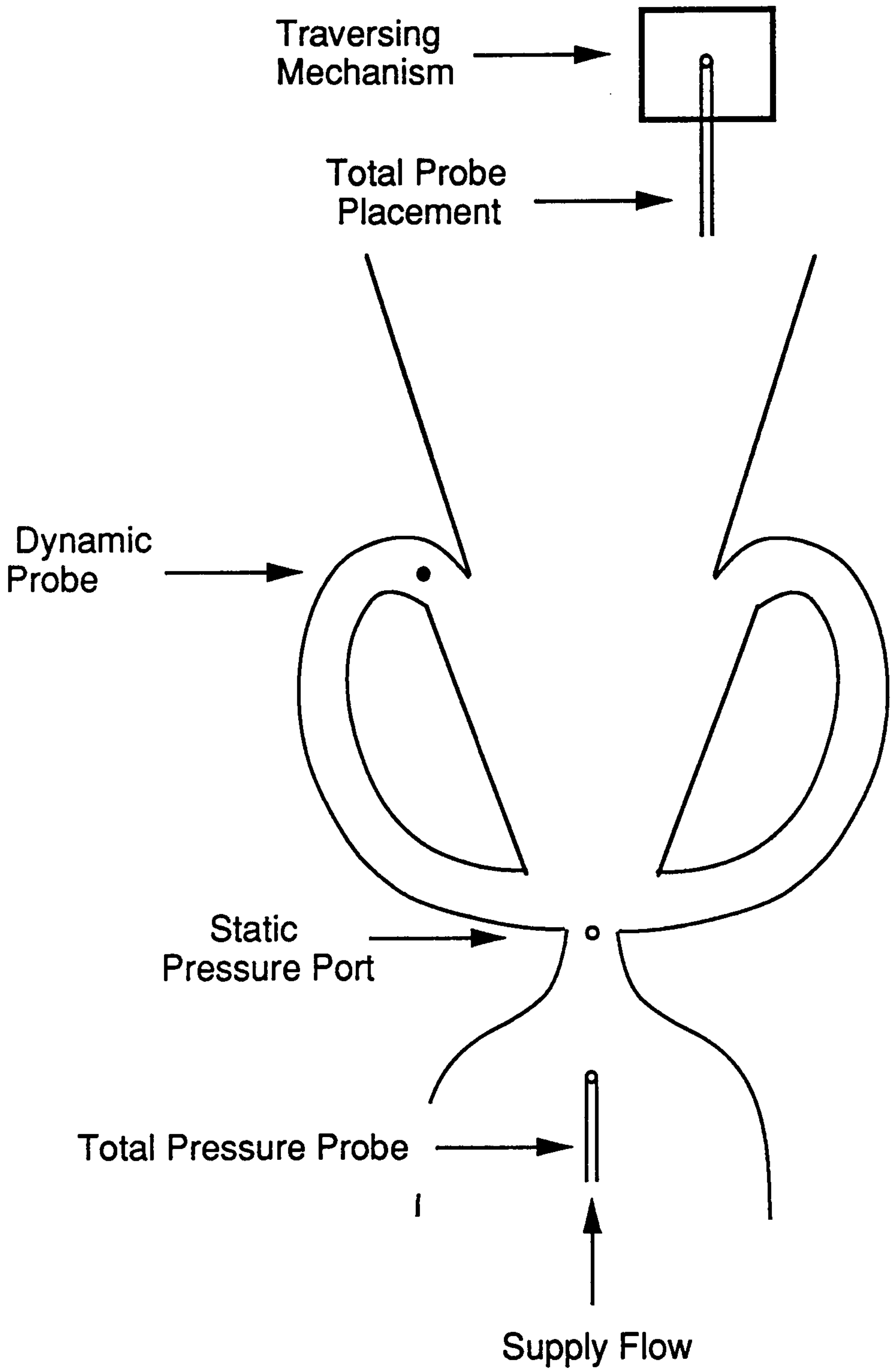

Figure 4.3. Instrumentation Used For Data Collection.

To visualize the flow, a surface oil flow technique was employed. This involved applying a matrix of paint dots to the surface of the model as the photograph of Figure 4.4 demonstrates. The paint was mixed with kerosene to enable the mixture to follow the flow more easily and to allow for the repeatability of the technique. When the model was provided with supply air flow, the paint that was spread in the direction of flow preserved the mean flow characteristics.

Results

In analyzing early experimental results, it was discovered that there existed an unsteadiness in the flow. By using the surface oil flow technique in the stilling chamber, it was discovered that the production of vortices from the flow negotiating the large turning angle from the air hose to the stilling chamber may have been asymmetric. The photographs in Figure 4.5 clearly illustrate the forming of a vortex in one corner of the stilling chamber while it is difficult to ascertain the present of a similar vortex in the other. To help resolve this problem, the corners of the stilling chamber were filled. While the flow angle may still have been very large, the effects of vortex production was reduced. The photograph in Figure 4.6 shows the flow field during the transition from the supply hose to the stilling chamber after the corners were filled. To further assist in straightening the flow provided to the supply nozzle, the two pieces of honey-comb in the stilling chamber were pushed together and a fine mesh screen was situated between them.

From the Spectrum Analyzer, frequency was recorded as nozzle supply flow rate was increased. A graph of frequency verses supply flow rate is provided in Figure 4.7. A linear relationship similar to that found in the water tunnel tests of the plexiglas model resulted. The highest frequency response recorded was $110Hz$ at a nozzle supply flow rate of $560ft^3/sec$ ($M \approx 0.98$). Unfortunately, this was the

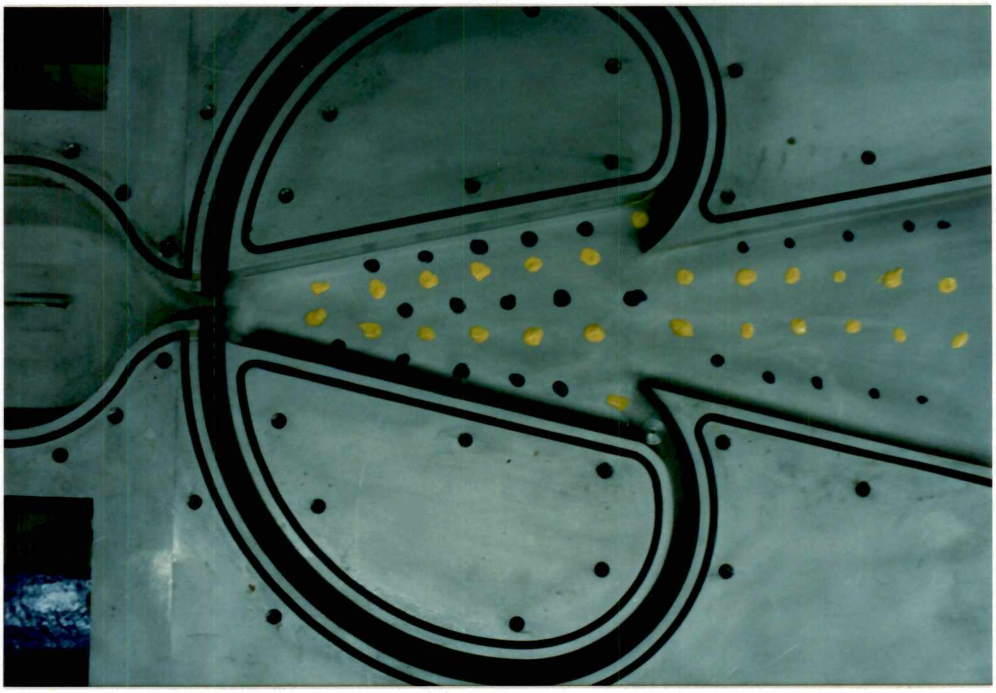

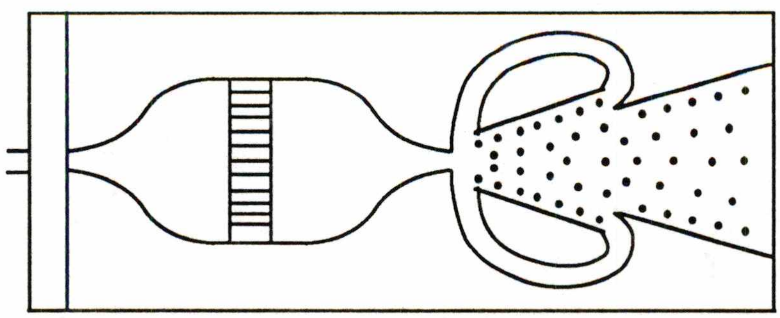

Figure 4.4. Typical Application Of Paint Dots Used In Surface Oil Flow Visualization Technique.

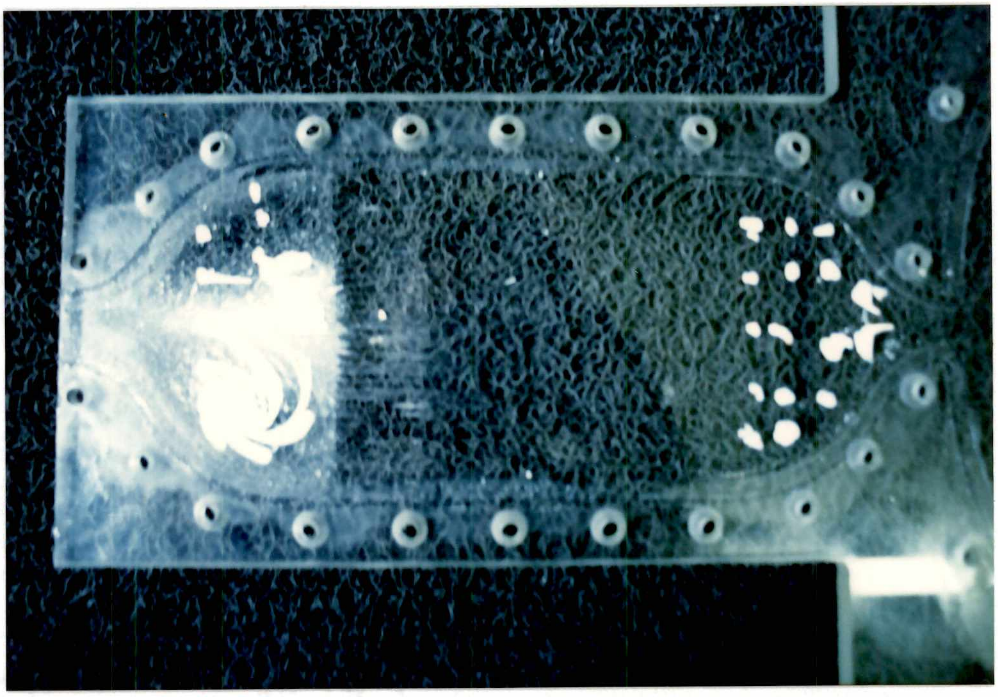

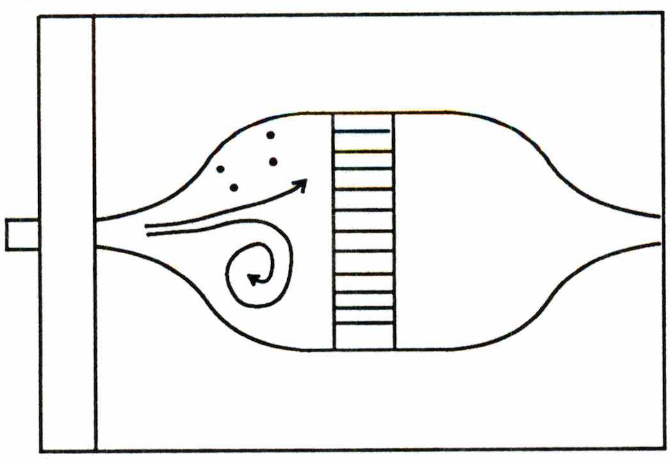

Figure 4.5. Asymmetric Forming Of Vortices In Stilling Chamber.

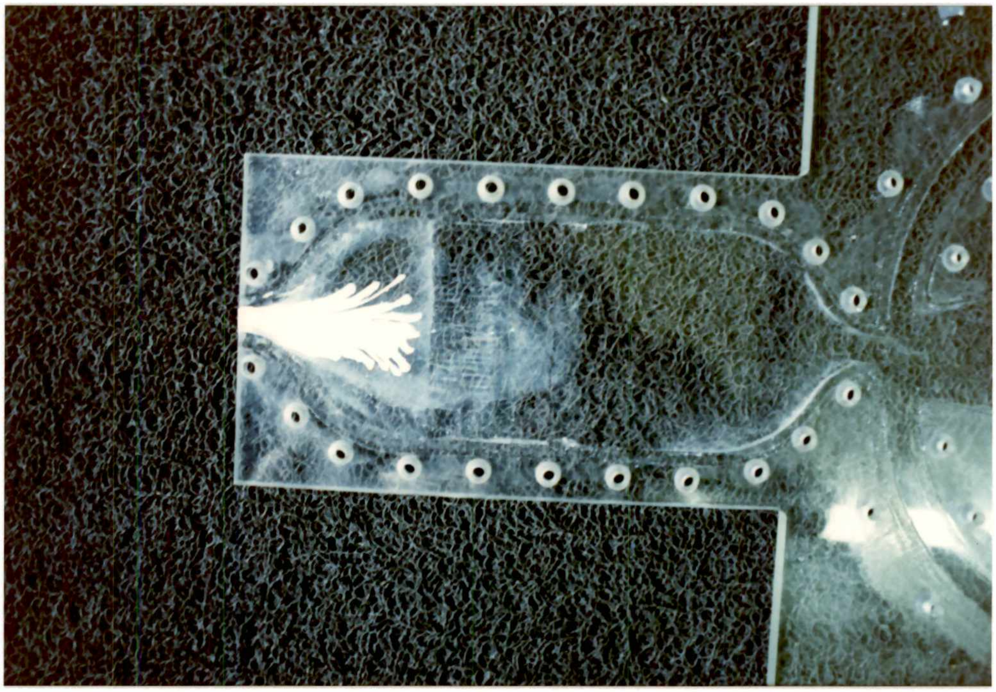

Stilling Chamber

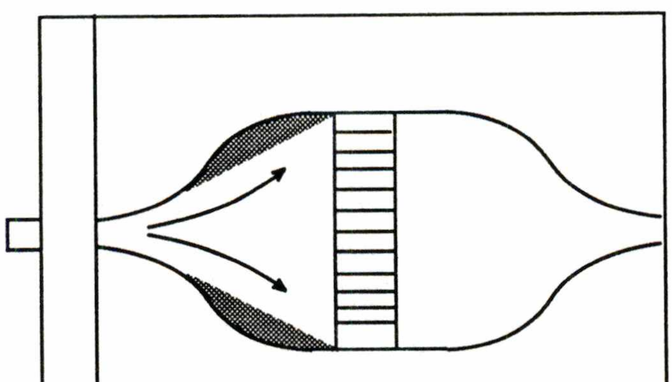

Figure 4.6. Flow Visualization Of Stilling Chamber After Corners Were Filled.

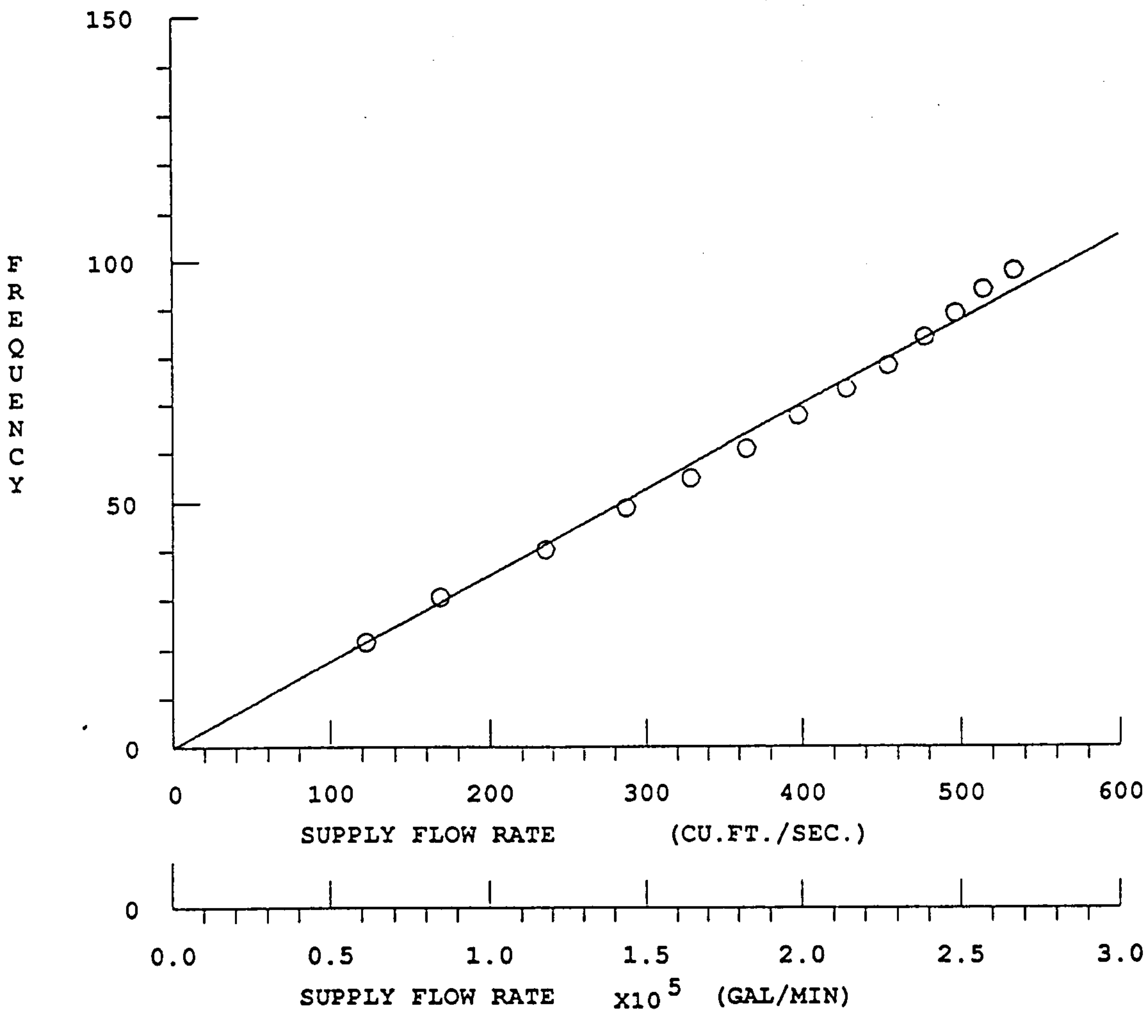

Figure 4.7. Characteristic Graph Of Frequency Verses Supply Flow Rate With Air As Medium.

limit attainable by the low pressure air hose.

In order to obtain a snapshot of the mean output conditions, the traversing mechanism was used to place the total probe at a fixed location across the exit plane. The fluidic device was operated at several different nozzle flow rates at each location. During the test runs, a six second burst of data was collected for each nozzle flow rate. The eight hundred pieces of data collected were then averaged and the mean value and standard deviation was recorded. From preliminary test results it was determined that the fluidic device provided a symmetrical output and so final test results are shown only for half the output. The test procedure was repeated for each quarter inch interval across the face of the output starting at one edge and terminating in the center. Referring to Figure 4.8, a graph of total pressure verses distance across the exit plane is provided for an increasing nozzle supply flow rate. To ensure accuracy of test results, the instrumentation was re-calibrated a number of times. The length of the tubing from the total probe to the pressure transducer was then minimized without an appreciable change in results. Finally, the total probe was exchanged for a dynamic pressure probe. The results showed many fluctuations in the output conditions but the mean values were consistent with the results obtained from the total probe. Overall, the results show that there is a significant loss in total pressure from the stilling chamber to the output conditions. These results are consistent with the studies of both Beale and Lawler[2] as well as S.M. Riddlebaugh.

To obtain a better understanding of the characteristics of the output flow, the surface oil flow visualization technique was employed. As previously discussed, a matrix of paints dots was applied to the base of the fluidic device. The photograph in Figure 4.9 illustrates the mean resultant flow behavior at a nozzle supply flow rate of $400 ft^3/sec$. It is evident from this picture that, as the fluid flows past the

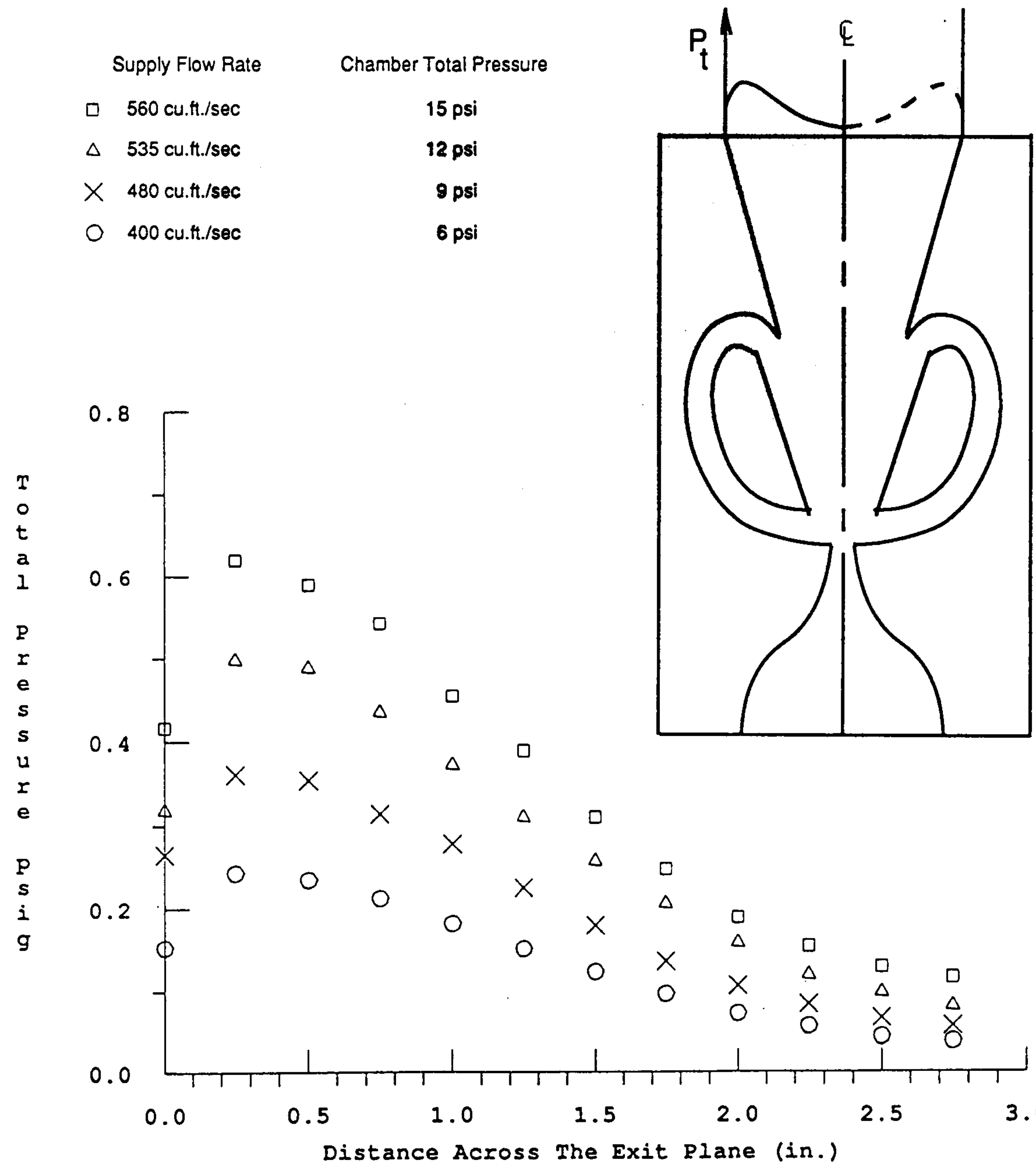

Figure 4.8. Output Characteristics Of One Half Of The Exit Plane With Varying Supply Flow Rate.

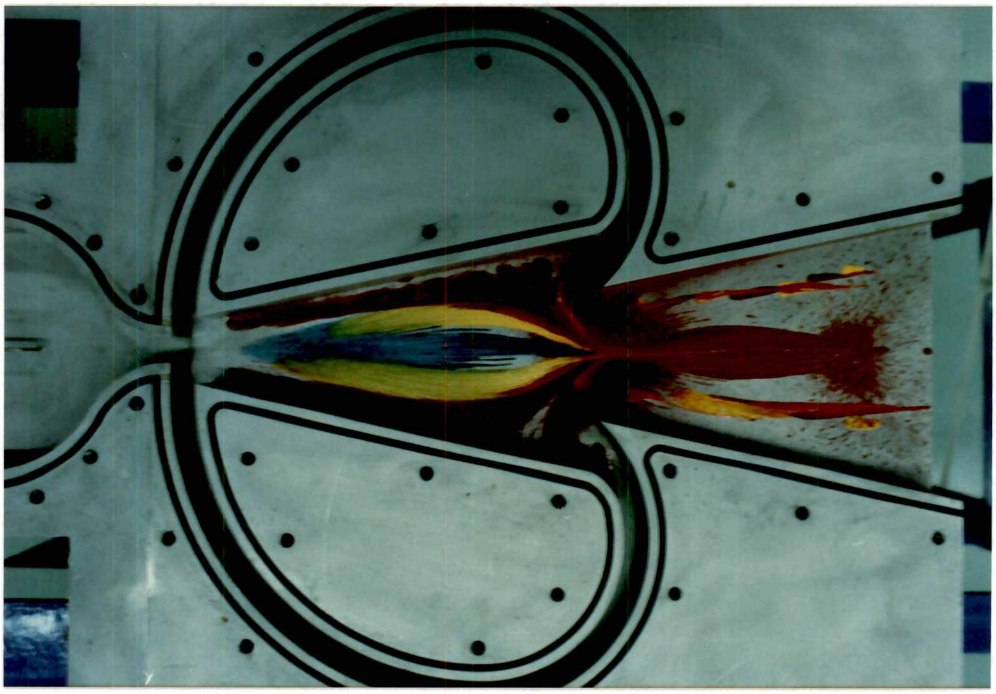

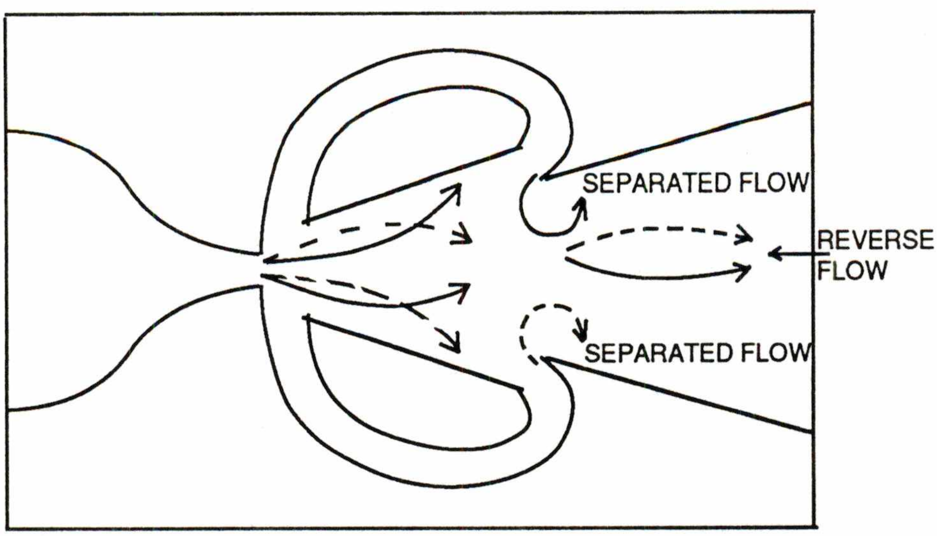

Figure 4.9. Flow Visualization Of Overall Flow Field.

entrance to the feedback loops, there is flow separation. The flow visualization was repeated for a nozzle supply flow rate of $200 ft^3/sec$ and $480 ft^3/sec$ with similar results. The supply nozzle is not yet choked so that it is unlikely that there are losses in the flow field due over-expansion. The separated flow is a major contributing factor to the loss in total pressure. The only other mechanisms for losses downstream of the nozzle are frictional effects and the unsteadiness in the flow that supports the fluid oscillations.

CHAPTER V

CONCLUSIONS AND RECOMMENDATIONS

The purpose for using wall attachment theory in this study was to assist the designing of a fluidic device that was suitable as an oscillator. Because of the design of the entrance to the feedback loops in the test model, the wall attachment point could have been anywhere prior to the entrance to the feedback loops and jet switching would have resulted. The ideal location for the wall attachment point, however, is the entrance to the feedback loops such that there is minimal time delay in transferring the fluid pulse that causes jet switching and hence, frequency of oscillation is optimized. To better apply the theory of wall attachment as has been presented in this study, a more indepth understanding of the relationship between the supply flow rate and the control flow rate is required. It has become profoundly obvious that the geometrical design of the entrance to the feedback loops dictates the amount of the supply flow captured in the feedback loops. It is recommended that a future study be undertaken to determine the relationship.

The results of the water tunnel test and the experimental proceedings with air have proven that a fluidic oscillator can, indeed, be used to provide a continuous pulsating output. From the two experiments, a linear relationship has been shown to exist between supply flow rate and frequency of oscillation. The highest frequency recorded in the air tests was $110 Hz$ with a supply flow rate of $560 ft^3/sec$ ($M \approx 0.98$). As has been previously discussed, however, the frequency of oscillation can be influenced by the volume of the feedback loops and so a higher frequency response can be obtained by merely modifying the feedback loops. Also, the test model was constructed to be large enough such that flow visualization was possible and instrumentation was feasible. The size of the model would affect the frequency of oscillation so that higher frequencies could be obtained with a smaller model. It is recommended that further studies be carried out on a scaled down version of this study's test model to determine the scaling relationship and the magnitude of frequency response obtainable.

Before any enthusiasm is generated for the use of fluidic oscillators in the desired application, there is a serious downfall in performance that must be corrected. The results of this study have shown a significant total pressure drop across the device. From analyzing the flow through visualization techniques, it appears that the method in which the entrance of the feedback loops were designed caused severe flow separation downstream of the feedback loops to the device's output. It would be of paramount importance to initiate a study on the existing model that examines better means of capturing the output such that the drop in total pressure across the device is minimized.

BIBLIOGRAPHY

BIBLIOGRAPHY

1. Vakili, A. D., et al., "Pulsed Jets in Cross-Flow," ASME, FED, Vol. 92, Edited by J. A. Miller and D. P. Telionis, June 1990, p.465-475

2. Beale, R. B. and Lawler, M. T., "Development of a Wall-attachment Fluidic Oscillator Applied to Volume Flow Metering," Vol. 1, Part 2, Instrument Society of America, 1974, p. 989-996

3. Riddlebaugh, S. M., "Use Of Fluidic Oscillator To Measure Fuel-Air Ratios Of Combustion Gases," NASA TM X-3068, Washington, D. C., June 1974

4. Delashmidt, Jr, W. H., "An Experimental Analysis of Feedback Effects in a Fluid Oscillator," Master Thesis, The University of Tennessee, March 1968

5. Humphrey, E. F. and Tarumoto, D. H., "Fluidics, Revised Edition," Fluid Amplifier Associates, Ann Arbor, Michigan, 1968.

6. Dohta, S. et al., "Jet Behavior In Wall-Attachment Fluidic Devices With Small Aspect Ratio," The Journal Of Fluid Control, New York, 1981

7. Kirshner, J. M. and Katz, S., "Design Theory Of Fluidic Components," Academic Press, Inc., 1975

8. Kinoshita, O. and Murakami, M., "The Characteristics of Curved Wall Power Fluidics," Engineering and Natural, Vol. 28, No. 1, 1978, p. 93-104

9. Romiti, A., "Fluid Dynamics Of Jet Amplifiers," Course Held At The Department Of Hydro and Gasdynamics, September 1970, Springer - Verlag Wien - New York, 1972

10. Bourque, C. and Newman, B. G., "Reattachment of a Two Dimensional Incompressible Jet to an Adjacent Flat Plate," Aeronautical Quarterly, Vol. XI, August 1960, p. 201

11. Friedman, S. B. and Martin, H. R., "Some Applications Of The Liquid-Jet Fluidic Device," ISA Transactions, Vol. 14, No. 1, 1975

12. Oshima, Y. and Kinoshita, O., "An Experimental Investigation Of The Water Jet In A Coanda Effect Fluidic Device," Proceeding Of IFAC 6th World Congress, Boston/Cambridge, MA, 24-30 Aug 1975

13. Goldstein, R. J., "Fluid Mechanics Measurements," Hemisphere Publishing Corporation, New York, 1983

APPENDIXES

APPENDIX A

```
C----------C-------------C------------C-------------C-------------C------
C
C                          FORTRAN PROGRAM
C
C----------C-------------C------------C-------------C-------------C------

      IMPLICIT REAL*8(A-H,O-Z)
      REAL LHS,N,M
C
C----------C-------------C------------C-------------C-------------C------
C
C     VARIABLES
C
C  A   - Angle Of Inclination Of the Attachment Wall
C  B   - Offset Distance From Nozzle To Side Wall
C  R   - Radius Of Curvature Of Flow Jet
C  RCS - Ratio Of Control Flow To Supply Flow
C  S2  - Distance Along Curved Jet Center Line Wall To Attachment Point
C  SE  - Spread Factor
C  TH  - Angle Extended Jet Center Line Makes With The Attachment Wall
C  XA  - Distance Along Wall To Attachment Point
C  YA  - Distance Perpendicular To Jet Axis Corresponding To Attachment
C        Streamline
C  W   - Power Nozzle Width (b)
C
C----------C-------------C------------C-------------C-------------C------
C
C     INPUT
C
      TYPE*,' PLEASE ENTER THE BASIC DIMENSIONS OF THE FLUIDIC DEVICE'
      TYPE*,' ENTER THE POWER NOZZLE WIDTH, b'
      READ(*,*)W
      TYPE*,' ENTER THE OFFSET DISTANCE FROM THE NOZZLE TO THE
     1SIDE WALL, B'
      READ(*,*)B
      TYPE*,' ENTER THE ANGLE OF INCLINATION OF THE ATTACHMENT
     1 WALL IN RADIANS, ALPHA'
      READ(*,*)A
      TYPE*,' ENTER THE ASSUMED SPREAD FACTOR, SIGMA'
      READ(*,*)SE
C
C
C----------C-------------C------------C-------------C-------------C------
C
       DO 400 J = 1,30
C
      RCS = J/100.
C
C----------C-------------C------------C-------------C-------------C------
C
C     NEWTON-RAPHSON ALGORITHM
C
      P = A + 0.01
C
       DO 100 I = 1,50
```

```
      LHS = DCOS(P + A)
      S = 0.5*DABS(DCOS(A))*(2*B + W)*(A + P)/
     1 (DABS(DCOS(A))-DABS(DCOS(P)))
      H = W*SE/3
      T = (1 + 2*RCS)*DSQRT(H/(S + H))
      RHS = 1.5*(T - ((T)**3)/3.)
C
C
      F = RHS - LHS
C
      PB = P
C
C
      P = P - F/4.
C
C
      ERR = DABS((P - PB)/P)
C
      IF(ERR.LT.0.0001) GOTO 200
C
C
 100  CONTINUE
C
C----------C-------------C------------C-------------C-------------C------
C
C
 200  TH = P
      S2 = 0.5*ABS(COS(A))*(2*B + W)*(A + TH)/(ABS(COS(A))-
     1 ABS(COS(TH)))
      R = S2/(A + TH)
      T = (1 + 2*RCS)*SQRT(H/(S2 + H))
      YA = 0.5*((S2 + H)/SE)*LOG((T + 1.)/(1. - T))
C
      XR = R*(ABS(SIN(TH)) + ABS(COS(TH))*ABS(SIN(A))) -
     1 YA/ABS(SIN(TH))
C
      XRW = XR/W
C
C----------C-------------C------------C-------------C-------------C------
C
C     OUTPUT
C
      WRITE(4,250) RCS,XRW
 250  FORMAT(1X,2F10.4)
C
 400  CONTINUE
C
C
      STOP
      END
```

APPENDIX B

Model Design Specifications

Design Parameter	Design Value
Off-Set Distance From Nozzle To Side Wall, B	0.25 in.
Supply Nozzle Width, b	0.50 in.
Width Of Feedback Loops, b	0.50 in.
Angle Of Inclination Of Attachment Wall, α	12 ^{o}
Aspect Ratio Of The Supply Nozzle	2
Spread Factor, σ_e	7.67
Length From Nozzle To Exit Plane	15.5 in.
Length From Nozzle To Feedback Loops	8.0 in.

VITA

Harry James Kowal was born on 8 May 1962 in Zwiebrucken, West Germany. His parents, Maurice and Jessie, live in Petawawa, Ontario, Canada. He graduated from Champlain High School, Pembroke, Ontario, Canada in 1980 after which he enrolled in the Regular Officer Training Plan of the Canadian Armed Forces.

His university education was achieved at the Royal Military College of Canada, Kingston, Ontario where he studied Mechanical Engineering. He was commissioned as an Officer in the Canadian Armed Forces in May 1984. To complete his training as an Aerospace Engineer, he attended the Canadian Forces School of Aerospace Engineering in Borden, Ontario.

Upon graduation, his first tour of duty was spent at National Defence Headquarters, Ottawa, Ontario where he served in the Directorate General of Aerospace Engineering and Maintenance as Life Cycle Material Manager for helicopter engines. During his stay, he became a Licensed Professional Engineer under the Association of Professional Engineers for Ontario.

In August 1988, he entered the University of Tennessee Space Institute for his post graduate education. In August 1990, he graduated with a Master of Science Degree in Aerospace Engineering.

Harry James Kowal is presently a Captain in the Canadian Armed Forces. He has a lovely wife, Cheryl Anne, who is a Registered Nurse. They have two wonderful daughters, Sarah Elizabeth and Stephanie Lynne.